JGR Atmospheres

RESEARCH ARTICLE
10.1029/2019JD031360

Key Points:
- Numerical model capable of reproducing the dynamics of negative-leader stepping and branching processes has been developed
- Model predictions on leader speed, step length, interstep interval, and charge transfer are in reasonably good agreement with observations
- Among other features current pulses generated at the end of step-formation process carry positive charge over hundreds of meters upward along the negative-leader channel

Supporting Information:
- Supporting Information S1
- Movie S1
- Movie S2
- Movie S3

Correspondence to:
A. A. Syssoev,
zaratustrann@yandex.ru

Citation:
Syssoev, A. A., Iudin, D. I., Bulatov, A. A., & Rakov, V. A. (2020). Numerical simulation of stepping and branching processes in negative lightning leaders. *Journal of Geophysical Research: Atmospheres*, *125*, e2019JD031360. https://doi.org/10.1029/2019JD031360

Received 18 JUL 2019
Accepted 27 FEB 2020
Accepted article online 3 MAR 2020

©2020. American Geophysical Union. All Rights Reserved.

Numerical Simulation of Stepping and Branching Processes in Negative Lightning Leaders

A. A. Syssoev[1,2], D. I. Iudin[1,2,3], A. A. Bulatov[1], and V. A. Rakov[4]

[1]Institute of Applied Physics of Russian Academy of Sciences, Nizhny Novgorod, Russia, [2]Department of Medical Physics and Informatics, Privolzhsky Research Medical University, Nizhny Novgorod, Russia, [3]National Research University Higher School of Economics, Moscow, Russia, [4]Department of Electrical and Computer Engineering, University of Florida, Gainesville, FL, USA

Abstract A numerical model with physical timing and grid spacing of 3 m is applied to studying the progression (including stepping and branching) of negative lightning stepped leader. The asymmetry between positive and negative streamers is taken into account via using polarity-dependent initiation and propagation field thresholds. The stepped nature of negative leader is confirmed to be caused by this asymmetry. The step formation process of the negative leader is modeled to begin with the appearance of space stems inside and in the immediate vicinity of its streamer zone (corona streamer burst completing the preceding step). Some of those space stems evolve into space leaders, which can connect to the primary leader channel, thereby facilitating its extension. Model-predicted morphology and dynamics of negative leaders are in good agreement with the recent recordings of lightning stepped and dart-stepped leaders obtained using high-speed video cameras, and their electrical parameters are in line with the current knowledge on negative lightning leaders.

1. Introduction

Since the 1930s, when Schonland and his coworkers have started their pioneering optical observations of negative leader development (see, e.g., Rakov & Uman, 2003, chapter 4, and references therein), it has been known that negative leaders in virgin air always develop in a stepped manner, with the step length being of the order of tens of meters and interstep intervals of the order of tens of microseconds. In contrast, positive leaders usually develop continuously. Significant progress has been made lately in understanding the step formation process using high-speed video (framing) camera records of rocket-triggered (Gamerota et al., 2014) and natural (Hill et al., 2011; Jiang et al., 2017; Lu et al., 2016; Petersen & Beasley, 2013; Qi et al., 2016; Tran et al., 2014) lightning. The recent observations with framing cameras yielded shorter step lengths and shorter interstep intervals, compared to earlier reports based on streak-camera records. The mechanism of step formation process in lightning appears to be similar to that observed in long negative sparks (Gorin & Shkilev, 1976; Ortega et al., 1994; Reess et al., 1995). However, many details of the step formation process remain unclear, including the genesis and evolution of the space stem, connection of the space leader to the primary leader channel, and generation of negative corona streamer burst. Bacchiega et al. (1994) simulated the negative stepped leaders in long laboratory sparks, whose sustained currents were a few amperes; that is, 1 to 2 orders of magnitude lower than negative leader currents in lightning. Carlson et al. (2015) and da Silva and Pasko (2015) modeled preliminary breakdown pulses in lightning with emphasis on reproduction of measured electric field waveforms. No space leaders were considered. Nag and Rakov (2016) simulated both the preliminary breakdown pulses and leader steps using a TL-type model. Cooray and Arevalo (2017), using a one-dimensional model of stepped leader development considering the processes in its streamer zone, estimated the step length, step formation time, and propagation speed of stepped leaders as a function of the prospective return stroke peak current. Zhang et al. (2017) presented a one-dimensional modeling study of the dynamics of branching of negative downward lightning leaders. Iudin et al. (2017) presented an advanced stochastic model of lightning development. They also reviewed other models of this type (see their Table 1).

The mechanism of negative leader stepping process is still poorly understood. It involves the formation of an active element (space leader) ahead of the primary leader channel tip. Bazelyan and Raizer (2000, p. 85) referred to the space leader emitting both positive and negative streamers as a “nearly mystic” phenomenon.

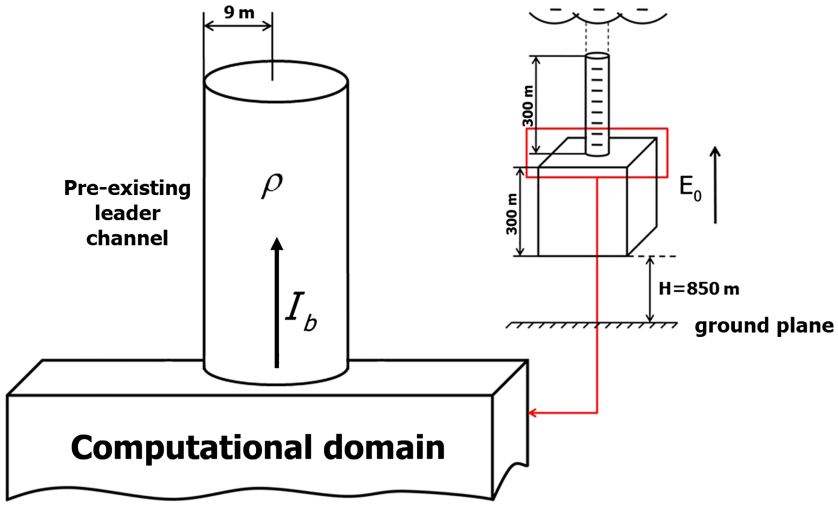

Figure 1. Cubical computational domain placed 850 m above ground level and the simulated preexisting leader channel attached to its top (not to scale). $\mathbf{E}_0$ is the electric field produced by cloud charges and their images, representing induced charges on the ground surface. The preexisting channel is negatively charged. Both cloud charges and preexisting channel charges contribute to the background potential distribution inside the computational domain. ρ is the line charge density of the preexisting leader channel, and I_b is the steady feeding current supplying negative charge to the leader channel developing inside the computational domain. In this study, ρ and I_b are assumed to be decoupled.

The available observations of stepping process are limited and do not provide sufficient physical insights. This is where modeling can help. Further, the lightning return stroke current largely depends on the charge distribution in the channel corona sheath. The corona sheath charge may originate from the streamer zone developing from the leader tip and from the radial corona from the lateral leader channel surface, the relative contributions from these two sources being presently unknown. Formation of the leader channel corona sheath is an intrinsic process in our model, although only one of its sources (streamer zone at the leader tip) is considered. Additionally, a better understanding of negative stepped leader propagation from the cloud to ground or to the grounded object is needed for improving lightning protection schemes.

In this work, which can be viewed as an extension of that of Iudin et al. (2017), we focus on the stepping and branching of descending negative lightning stepped leader. In contrast with previous studies, we consider all the stages of step formation process (including space leaders) in a stochastic procedure, which necessarily makes the number of adjustable parameters large. We do perform the sensitivity analysis and compare our model predictions with the available observations.

Specifically, we compare the results of our simulations with time-resolved optical records of lightning (Hill et al., 2011; Jiang et al., 2017; Lu et al., 2016; Petersen & Beasley, 2013; Qi et al., 2016; Tran et al., 2014) and sparks (Gorin & Shkilev, 1976; Ortega et al., 1994; Reess et al., 1995), which are considered most informative to date. We also compare our model predictions with the various parameters of negative lightning leaders found in the literature, including the leader speed, step length, interstep interval, and step charge transfer. All these observations and parameters serve as constraints for our model, which is the first attempt to stochastically reproduce the competition between direct propagation of the negative leader and its extension via development of space leader.

2. Model Description

2.1. General Configuration

Morphology and development of stepped leader in negative lightning are modeled in the Cartesian space region having the shape of a cube with an edge of 300 m. This cubical volume is divided into $3 \times 3 \times 3$ m^3 cells, so that the spatial resolution (grid spacing) of our model is equal to 3 m. The center of the cubical computational domain is located at a height of 1 km above the ground level. This altitude approximately corresponds to the heights, at which lightning leaders were recorded using high-speed video cameras (see, e.g., Hill et al., 2011; Petersen & Beasley, 2013; Qi et al., 2016). Note that, because of the relatively weak dependence of air pressure (and, hence, reduced electric field) on altitude in the lower troposphere, the

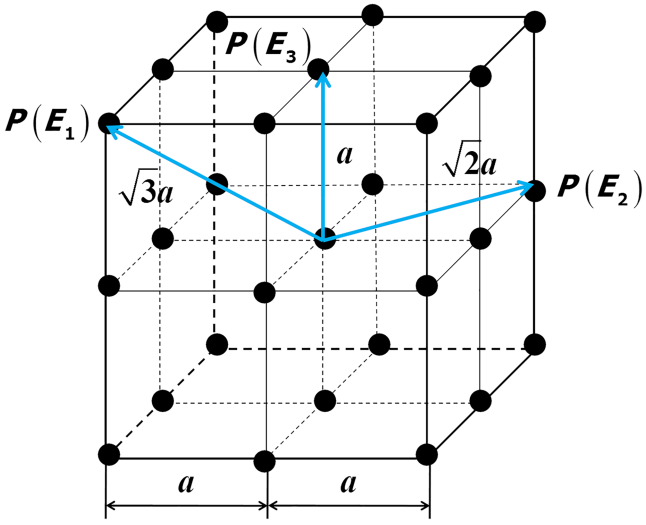

Figure 2. Illustration of different directions (a total of 26, three of which are shown by blue arrows) available for discharge extension in the three-dimensional computational domain (grid nodes are represented by black circles). $P(E_1)$, $P(E_2)$, and $P(E_3)$ are the breakdown probabilities, given by equation (5), corresponding to the three blue arrows, whose lengths are $\sqrt{3}a$, $\sqrt{2}a$, and a, respectively.

use of, for example, 0.5 or 2.0 km would not significantly change the discharge dynamics. A vertical uniformly charged cylinder whose length and radius are 300 m and 9 m, respectively, is attached to the top of the computational domain, as shown in Figure 1. This cylinder simulates the previously created leader channel, whose lower end just arrived at the top of the computational domain. Thus, what we simulate in the present study is only the lower end of the descending negative leader. The background potential distribution is determined by (1) a constant, upward directed electrical field $\mathbf{E}_0$ produced by cloud charges and (2) negative charges deposited on the previously created channel. Image charges (due to the presence of ground) also contribute to the potential distribution. Figure 2 shows all possible directions of discharge extension.

The bulk of the preexisting leader channel charge is assumed to reside in the corona sheath whose radius is expected to be of the order of meters or more, which is much larger than the millimeter-scale radius of the channel core (e.g., Rakov & Uman, 2003, pp. 134-135). The line charge density ρ of the preexisting channel is set to 800 μC/m. The line charge on the cylinder axis is 132 μC/m, and it is assumed to decrease as inverse radial distance r from the axis (the distinction between the channel core and corona sheath is neglected), which corresponds to the assumption of constant radial electric field in the corona sheath (Bazelyan & Raizer, 2000, p. 69). The magnitude E_0 of the electric field produced by cloud charges (and their images) is assumed to be 30 kV/m, which is expected at an altitude of 1 km above ground level (MacGorman & Rust, 1998, p. 53). In order to supply negative charge to the developing leader channel inside the computational domain we used feeding current I_b (where "b" stands for the upper boundary of computational domain). Three values of I_b, 100, 200, and 300 A, which are expected for negative lightning stepped leaders (see Rakov & Uman, 2003, chapter 4, and references therein), were used. Current I_b was assumed to flow along the z axis and be decoupled from the background charge density distribution within the cylinder.

The most significant model parameters, as well as the reasoning behind their choice (including sensitivity analysis) are presented in Table S1 and Text S6 in the supporting information.

2.2. Electric Potential and Electric Field Distributions

Electric potential φ, produced by both constant electric field $\mathbf{E}_0$ and point charges (and their images) located both at the grid nodes of the computational domain and outside the computational domain, can be calculated as the solution of Poisson's equation. In this study, the potential is calculated using the following expression:

$$\varphi(\mathbf{r}) = \frac{1}{4\pi\varepsilon_0}\left(\sum_{\mathbf{r}'\neq\mathbf{r}}\left\{\frac{q_{r'}}{|\mathbf{r}-\mathbf{r}'|} - \frac{q_{r'}}{|\mathbf{r}_\perp - \mathbf{r}'_\perp + (2H + z' + z)\mathbf{z}_0|}\right\} + \frac{q_r}{a/2} - \frac{q_r}{2(H+z)}\right) + \varphi_0, \quad (1)$$

where q_r and $q_{r'}$ are charges located at the space grid nodes with radius vectors $\mathbf{r}=\{\mathbf{r}_\perp, z\}$ (observation point; the last two terms in the parentheses) and $\mathbf{r}'=\{\mathbf{r}'_\perp, z'\}$ (source points; the first two terms in the parentheses), respectively, ε_0 is the electric permittivity of vacuum, $a/2 = 1.5$ m ($a = 3$ m is the grid spacing) in the next to the last term in the parentheses is the fictitious distance which is needed between the source and observation point to avoid singularity, $H = 850$ m is the height of the lower boundary of the computational domain above ground, which corresponds to $z = 0$, $\mathbf{z}_0$ is the upward directed unit vector of the z axis, and φ_0 is the background potential associated with the cloud charges (specified via constant electric field $\mathbf{E}_0$) and charges deposited on the previously created channel. The summation in formula (1) is performed over all the grid nodes and their images (ground is assumed to be perfectly conducting), except for the one at which the potential is calculated. In the latter case, the node potential is estimated as its charge divided by one-half of the grid spacing and the corresponding image node potential as its charge divided by $2(H + z)$ (see the last two terms in the parenthesis). The background potential φ_0 at each grid point was specified as

$$\varphi_0(\mathbf{r}) = \frac{1}{4\pi\varepsilon_0}\sum_{\mathbf{r}'}\left\{\frac{q_{r'}(\mathbf{r}'_\perp)}{|\mathbf{r}-\mathbf{r}'|} - \frac{q_{r'}(\mathbf{r}'_\perp)}{|\mathbf{r}_\perp - \mathbf{r}'_\perp + (2H + z' + z)\mathbf{z}_0|}\right\} - E_0 z, \tag{2}$$

where summation is performed over all the nodes with radius vectors $\mathbf{r}'=\{\mathbf{r}_\perp{}', z\}$ belonging to the preexisting leader channel with radius $R = 9$ m and containing point charges, magnitudes of which are independent of z and are specified as

$$q_{\mathbf{r}_\perp} = \begin{cases} q_0, & \mathbf{r}_\perp = \mathbf{r}^0_\perp \\ \frac{q_0 \cdot (1\text{ m})}{|\mathbf{r}_\perp - \mathbf{r}^0_\perp|}, & 0 < |\mathbf{r}_\perp - \mathbf{r}^0_\perp| \le R \\ 0, & |\mathbf{r}_\perp - \mathbf{r}^0_\perp| > R \end{cases}, \tag{3}$$

where $q_0 = 397\,\mu$C is the magnitude of each of the point charges at the preexisting leader channel vertical axis with $\mathbf{r}_\perp = \mathbf{r}^0_\perp$. It is assumed that the previously created channel contains the nodes of Cartesian coordinate system (upward extension of the computational domain), which are enclosed by a cylindrical surface specified by $1,150 < z[\text{m}] < 1,450$ and $0 \le |\mathbf{r}_\perp - \mathbf{r}^0_\perp| \le R$ (see Figure 1).

Note that the point charge self-contribution to electric potential in our equation (1) is consistent with the general approach used in numerical techniques to avoid singularities (e.g., Sadiku, 2018, quation 14.39 on p. 783) and that equations (1) and (2) (also employed by Iudin et al., 2017) automatically ensure that the electric potential at both the ground plane and at infinity is equal to 0. Therefore, no explicitly specified boundary conditions are needed.

The electric field strength $\mathbf{E}_{r,r'}$ between two grid nodes with radius vectors $\mathbf{r}$ and $\mathbf{r}'$ is calculated as

$$\mathrm{E}_{r,r'} = \frac{-(\varphi(\mathbf{r}) - \varphi(\mathbf{r}'))}{L}\frac{\mathbf{r}-\mathbf{r}'}{|\mathbf{r}-\mathbf{r}'|}, \tag{4}$$

where $L = \left\{(6 + 12\sqrt{2} + 8\sqrt{3})/26\right\} a \approx 4.25$ m is the average length of 26 possible paths of discharge growth (see Figure 2), which we used to avoid the dealing with different lengths (ranging from a to $\sqrt{3}a$) of extension paths available in the model. This approach gives some preference to diagonal paths, but the resultant bias does not materially influence the main conclusions of the present study.

2.3. Electric Fields Required for Discharge Initiation and Propagation

In this work, we will deal with both creation of floating channel segments and extension of existing channels. In either case, the bridging of neighboring nodes of the grid will occur. Any new link necessarily has a low initial conductivity characteristic of streamer formations ($\sigma_0 = 10^{-5}$ S/m or so [Maslowski & Rakov, 2006]). A streamer link, which can be viewed as a "streamer system" (Phelps, 1974) or "collective streamer" (Luque & Ebert, 2014), will either decay or make transition to a leader link, if its conductivity exceeds a threshold value assumed here to be 1 S/m. Leader links (except for the initial one) are also each a subject of decay. For lightning leader channels, the conductivity is of the order of 10^4 S/m (Rakov & Uman, 2003; Table 4.9). Leader links that do not decay are responsible for the growth of the discharge tree, while all the decayed links serve to redistribute the space charge.

A necessary condition for a new floating link creation is that the electric field between two neighboring nodes exceeds the initiation threshold value. If the discharge has already started, its further development

requires electric field exceeding the propagation threshold value, which is considerably lower than the initiation one.

Initiation E_{ith} and propagation E_{pth} threshold fields in numerical models of lightning development depend on grid spacing and, hence, should be viewed as effective (e.g., Iudin et al., 2017; Mansell et al., 2002). In this study, we assume a factor of 2 different threshold fields for positive (superscript "+") and negative (superscript "-") polarities: $E^+_{ith} = 1.34$ MV/m, $E^-_{ith} = 2.68$ MV/m, $E^+_{pth} = 0.31$ MV/m, and $E^-_{pth} = 0.62$ MV/m at an altitude of 1 km, which corresponds to the height of our computational domain center above ground level. Similar streamer propagation fields were obtained experimentally by Allen and Mikropoulos (1999) and theoretically estimated by Gallimberti et al. (2002) for positive polarity and adopted for both polarities in a number of lightning development models (Iudin & Davydenko, 2015; Iudin et al., 2015, 2017; Mansell et al., 2010, Tan et al., 2006). Note that in this study E^+_{ith} and E^-_{ith} apply only to the initiation of first collective streamer from the node representing the space stem and that, because of $E^-_{ith} > E^+_{ith}$, the first streamer is always positive and, hence, E^-_{ith} is not needed in modeling the initiation of streamers from the space stem. Further, we used reduced initiation threshold fields $E^+_s = 0.67$ MV/m and $E^-_s = 0.81$ MV/m for subsequent (secondary) positive and negative collective streamers (discussed below) initiated from the space stem, respectively. Note that, as we use a relatively small grid spacing of 3 m, the threshold fields values employed in our model are significantly higher than that used in other numerical lightning models (e.g., Iudin et al., 2017; Mansell et al., 2002).

Streamer links are relatively cold and have relatively large cross-sectional dimensions. In contrast, leader links are expected to have narrow (radii of the order of 1 mm) cores surrounded by large corona sheaths, with the core temperature being of the order of thousands of Kelvin (of the order of 10^4 K for lightning stepped leaders; Rakov and Uman, 2003, p. 7). The transition of an individual streamer to leader is outside the scope of this study. We assume here that the transition of a streamer link, which is a multitude of branched and interacting streamers, to leader link occurs gradually, as a result of increasing the energy input into the link.

For the case of extension of existing channel, the stochastic nature of discharge development is implemented via the probability distribution function which gives the discharge probability in a given direction, taking into account both the initiation (E_{ith}) and propagation (E_{pth}) thresholds. The probability of bridging a pair of grid nodes with the radius vectors $\mathbf{r}$ and $\mathbf{r}'$ is given by

$$P(E_{r,r'}) = \begin{cases} 1 - \exp\left[-\left|\frac{E_{r,r'} - E_{pth}}{E_{ith}}\right|^m\right], & E_{r,r'} \geq E_{pth} \\ 0, & E_{r,r'} < E_{pth} \end{cases}, \quad (5)$$

where m is the index determining the steepness of the breakdown probability function (based on the previous modeling experience, we set $m = 2$ in this study). This probability is 0 if the electric field strength E between two adjacent nodes is below the corresponding propagation threshold and increases with increasing E. An overview of the discharge growth probability functions employed in different models is found in work of Iudin et al. (2017). Expression (5) also applies to the case of new floating channel formation, provided that E_{pth} is replaced with E_{ith} (initiation of the first (positive) streamer link from the space stem) or E_s (initiation of subsequent (positive or negative) streamer link from the space stem). As noted above, the initiation of the first negative streamer link from the space stem is not considered in this study. The discharge probability function (5) is graphically shown in Figure 3 for the following five cases: initiation of the first positive streamer channel (E^+_{ith}) and subsequent positive (E^+_s) and negative (E^-_s) streamer channels, all from the space stem, and extension of existing positive (E^+_{pth}) and negative (E^-_{pth}) channels. Note that $E^+_{pth} < E^-_{pth} < E^+_s < E^-_s < E^+_{ith}$, with

$$\begin{cases} E^-_{pth} = 2 \times E^+_{pth} \\ E^-_s = 1.2 \times E^+_s. \end{cases} \quad (6)$$

The use of reduced thresholds E_s for subsequent streamer initiation in our model allowed us to reproduce the experimentally observed (e.g., Gorin & Shkilev, 1976; Ortega et al., 1994; Reess et al., 1995) negative streamer initiation from space stems. If we employed only two thresholds, E_{pth} and E_{ith}, there would be a vanishingly small number of negative streamers originating from the space stem. Physically, the reduced thresholds for secondary streamers, $E_s < E_{ith}$, can be explained by polarization and elongation of the space stem after the first streamer initiation. The elongation of space stem along the local electric field should lead

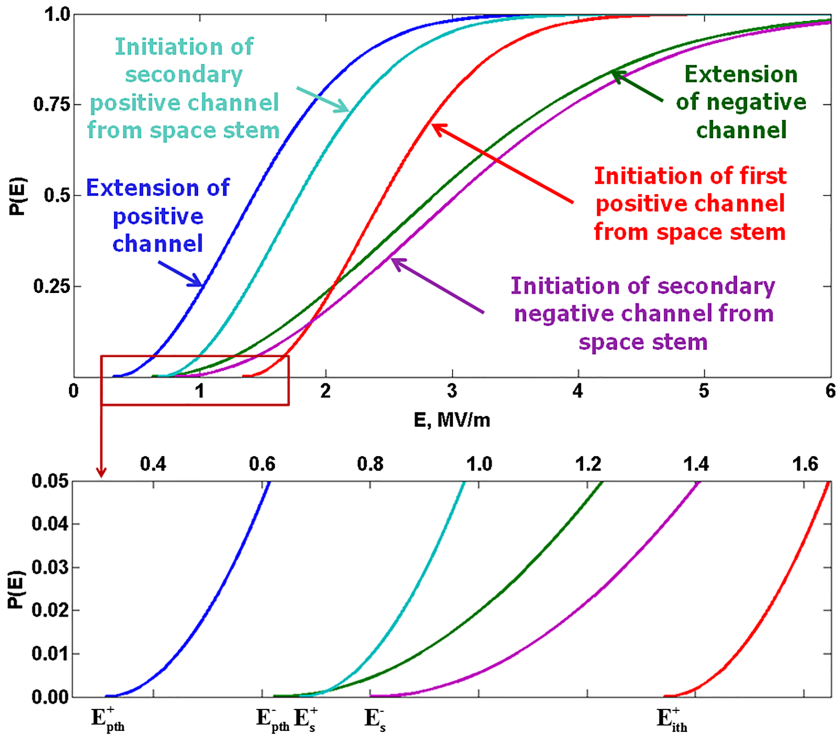

Threshold fields

E^+_{pth}, MV/m	E^-_{pth}, MV/m	E^+_s, MV/m	E^-_s, MV/m	E^+_{ith}, MV/m	E^-_{ith}, MV/m
0.31 (1.43)	0.62 (2.86)	0.67 (1.79)	0.81 (3.04)	1.34 (2.46)	2.68 (4.92)

Figure 3. The discharge probability functions (top panel) and their enlargements to better show the threshold fields (bottom panel) given by equation (5) for the cases of extension of existing positive and negative channels, as well as for three other cases corresponding to the initiation of first positive channel from the space stem (when E_{pth} in equation (5) is replaced with E^+_{ith}) and initiation of subsequent (secondary) positive and negative channels (when E_{pth} in equation (5) is replaced with E^+_s or E^-_s, respectively). The field thresholds are marked in the bottom panel (the corresponding text labels are found in the top panel) and their values are given in the table, below the plots, with 50% fields (corresponding to $P(E) = 0.5$) being given in the parentheses. The discharge probability function for initiation of first negative channel from the space stem is not shown, because the first streamer initiated from the space stem is always positive, but the value of E^-_{ith} is given (for completeness) in the table.

to reduction of effective electric field needed for initiation of secondary streamers from the space stem. Note that, in contrast with E_{pth}, $E^-_s \neq 2E^+_s$. This was needed to limit the number of positive streamers originating from the space stem. Without such limitation the number of secondary positive streamer links originating from the space stem would be unreasonably large.

Using the trial-and-error approach, we attempted to reduce the number of thresholds in our model but found that all of them were necessary for reproduction of the observed features of negative stepped leaders. This finding is related to the large number of processes involved in leader stepping, which we try to reproduce as closely as possible. In other words, the large number of thresholds (and other adjustable parameters) in our model is commensurate with the complexity of the processes being modeled.

2.4. General Leader Development Algorithm

The overall leader discharge tree develops as described next, with the simulated leader stepping mechanism being described in Appendix C. At each time step, any node belonging to the positive or negative part of discharge tree can create a positive or negative link, respectively, with any neighboring node of the grid, which does not belong to the part of discharge tree of the same polarity, with the probability given by formula (5). The only exception are nodes simulating space stems, which can produce links of both polarities. Creation of a link originating from the existing discharge tree is referred to here as propagation. Further, any free node can give rise to a new floating positive link with a neighboring node. Creation of such a link is called here initiation and the node giving rise to this link is designated a space stem. It is worth noting that, in principle, a positive streamer link can bridge nodes belonging to the primary negative leader streamer zone. The algorithm does not allow formation of loops in the discharge tree.

The basic element of the discharge tree is the conducting link, which represents a discharge channel (initially a low-conductivity streamer formation that may or may not make transition to a leader channel) between a pair of nodes. Peripheral links of the tree are more likely to remain at the streamer stage and decay. Negative streamer channels belonging to the primary negative leader streamer zone never make transition to the leader stage and eventually decay.

A newly formed link facilitates charge transfer between the two nodes it connects. When positive charge is transferred to one of those nodes, equal amount of negative charge is placed at the other one and vice versa. The magnitude of charge transferred between two adjacent nodes with radius vectors $\mathbf{r}$ and $\mathbf{r}'$ is found as $\delta q_{r,r'} = \alpha E_{r,r'}$, where α is set (using the trial-and-error approach) to 5.03×10^{-12} C × m/V. As an example, for electric field values, under which channel extension probability $P(E)$ is 0.5 (50%) (see Figure 3), charges separated by a newly formed streamer link are 7.2 and 14.4 μC for positive and negative polarity, respectively. Physically, parameter α depends on the properties of newly formed streamer link, such as its cross-sectional area and conductivity.

Channel conductivity σ varies by orders of magnitude as its temperature increases due to Joule heating and then decreases due to cooling processes (dependence of σ on temperature and pressure is given by Yos, 1963). In our model, we do not consider the detailed temperature dynamics and use a simple parametrization of the evolution of channel conductivity, which is given by the following equation:

$$\frac{\partial \sigma}{\partial t} = (\eta E^2 - \beta)\sigma, \tag{7}$$

where η and β are parameters that represent the rates of channel heating and cooling, respectively. Such parametrization is widely used in the models of the type employed in this study (e.g., Dulzon et al., 1999; Iudin et al., 2017; Rompe & Weizel, 1944). We used the following recurrent form of equation (7), written for a pair of nodes with radius vectors $\mathbf{r}$ and $\mathbf{r}'$:

$$\sigma_{r,r'}(\tau + 1) = \left\{1 + (\eta' E_{r,r'}^2 - \beta')\right\} \sigma_{r,r'}(\tau), \tag{8}$$

where $\sigma_{r,r'}(\tau)$ and $\sigma_{r,r'}(\tau + 1)$ are the conductivity values at the current and the following steps of the computational procedure, respectively, $\eta' = \eta\tau$, $\beta' = \beta\tau$, and $\tau = 2.12$ μs is the model time step averaged over all possible discharge tree growth directions (see Figure 2). More details on the temporal evolution of channel conductivity in our model and in other models of this type can be found in work of Iudin et al. (2017). In this study, parameter η', responsible for channel conductivity increase, is assumed to be constant and set (using the trial-and-error approach) to 6×10^{-13} m$^2/V^2$, while parameter β' determining the rate of conductivity decrease at step $(\tau + 1)$ is expressed as a function of channel conductivity at step τ:

$$\beta'_{r,r'}\left(\sigma_{r,r'}(\tau)\right) = 10^{-5}\left\{1 + \exp\left(\frac{\sigma_{r,r'}(\tau)}{\bar{\sigma}}\right)\right\}, \tag{9}$$

where $\bar{\sigma} = 10^4$ S/m is the expected conductivity of hot leader channel core. The initial value of newly formed channel conductivity σ_0 is set to 10^{-5} S/m, which is close to the expected conductivity of streamer formations (e.g., Maslowski & Rakov, 2006). Since for an arc in air at pressures ranging from 1 to 10 atmospheres and temperatures higher than 1.5×10^4 K or so the conductivity doesn't vary much and remains of the order of 10^4 S/m (see, e.g., Rakov, 1998, and references therein), we limit the model channel conductivity to 2×10^4 S/m. Equation (9) is a semiempirical one; it was developed using the trial-and-error approach.

Note that the link (channel) in our model is a virtual object. One can view it as a rectangular slab or as a thin cylinder, and the only parameter that depends on the cross-sectional area is conductivity. The slab conductivity related to its cross-sectional area S, which can be equal to a^2, $(\sqrt{2}a)^2$ or $(\sqrt{3}a)^2$ depending on link orientation (see Figure 2), can be scaled to the corresponding physical conductivity of an equivalent link, carrying the same current, but via a realistic (much smaller in the case of leader channel) cross-sectional area πr^2, where r can be viewed as the actual radius of current-carrying channel, by multiplying it by $S/(\pi r^2)$. In this study, we assumed (see Appendix B) that the channel radii of links belonging to the main negative leader structure with feeding currents I_b of 100, 200, and 300 A are 0.56, 0.80, and 0.98 mm, respectively, while the radii of channels belonging to space streamers/leaders are 0.20 mm, regardless of I_b. As an approximation, all links in the model can be viewed as having the same (average) slab cross-sectional area $S = L^2 = 18.1\ \mathrm{m}^2$, where L=4.25 m is the average link length.

The electric field along a link is found as the potential difference between the nodes at its ends divided by the length of the link (L). This field gradually relaxes from the prebreakdown value to the hot-channel value (if the transition from streamer link to leader link takes place) of 10^4 V/m (Mansell et al., 2010) under the action of potential equalization by currents flowing through all the discharge tree channels (Iudin et al., 2017). For each link, joining nodes with radius vectors $\mathbf{r}$ and $\mathbf{r}'$, this current is found from Ohm's law as

$$I_{r,r'} = \sigma_{r,r'} \pi r^2 E_{r,r'}. \tag{10}$$

The field-relaxation currents given by (10) lead to polarization of the entire conductive discharge tree in the overall electric field in the computational domain and to charge accumulation at the channel branch tips. This means that the electric field decreases in the interior of the discharge tree with its simultaneous intensification at the discharge tree periphery (Iudin et al., 2017).

The method of supplying negative charge to the growing discharge tree in our model is described in Appendix B.

As noted above, it is assumed in this study that any newly added channel segment is initially a low-conductivity ($\sigma = 10^{-5}$ S/m) streamer formation, which can be transformed, via Joule heating, into a well-conducting leader channel. In order to facilitate leader stepping, we limited the conductivity of all new channel segments originating from the negative leader tip by capping their conductivity at 1 S/m regardless of current they carry. This value is typical for both the streamer head (Raizer, 2009) and for the newly formed positive laboratory leader channel carrying a current of 1 A (Raizer, 2009, p. 602) but is much lower than the conductivity of lightning leaders (Rakov & Uman, 2003, p. 164). Our approach, in effect, would prevent continuous propagation of the primary negative leader, which in principle may occur, but is unlikely. On the other hand, conductivity of streamer channels of either polarity developing from space stems was not limited and they were allowed to evolve into leader channels. Possible propagation of space stem between steps (see, e.g., Gorin & Shkilev, 1976) was neglected.

Most space streamers never become space leaders and, hence, do not produce steps. If the first positive streamer channel initiated from the space stem comes in contact with the negative leader channel, it is removed with the separated space charges being conserved. We refer to such space stems creating "premature" streamer connection to the primary leader channel as "failed space stems." Further, some discharge tree branches (even if their conductivity exceeds 1 S/m) may stop growing, lose connection with the main discharge tree, and decay. The charge previously transported to the node corresponding to the decayed branch tip (or to both tips if the decaying structure is a single floating link) remains "frozen" at that node (or nodes), because of the low conductivity of the medium and the relatively small time (compared to the charge relaxation time) needed for the discharge development (see Table C1). These "frozen" charges contribute to the formation of the leader corona sheath (see, e.g., Bazelyan and Raizer, 2000, Figure 2.2). As noted in section 1, another contributor to the corona sheath is the radial corona current (see, e.g., Maslowski & Rakov, 2006) from the channel core, which is not considered in our model.

If a branch does not generate any new links, the probability of its decay (extinction) depends on its conductivity σ and is generally given by

$$P_d(\sigma) = 1 - \tanh(\sigma/\sigma_m), \tag{11}$$

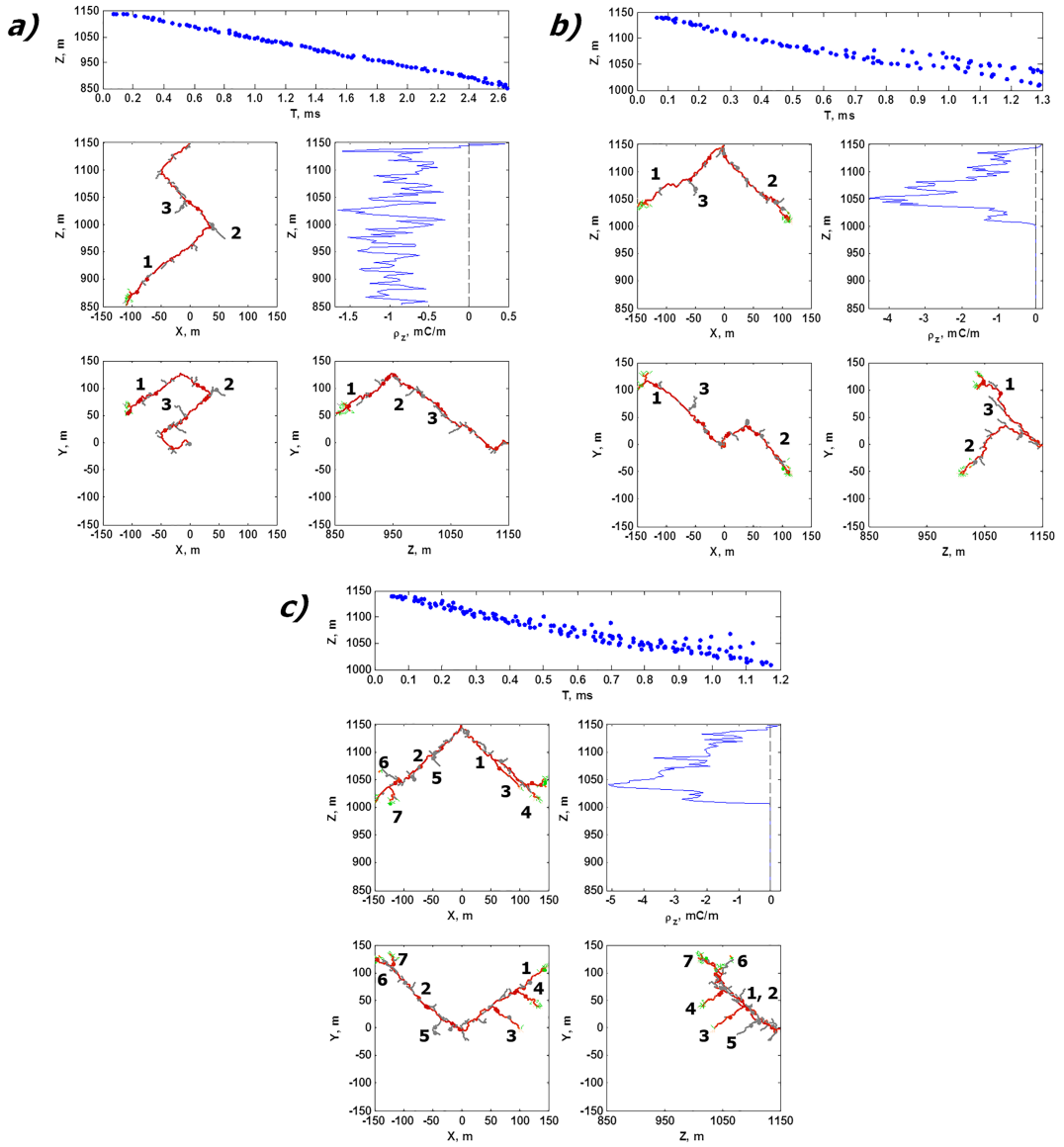

Figure 4. Two-dimensional projections onto the *x*-*y*, *x*-*z*, and *y*-*z* planes of three modeled negative stepped leaders with feeding currents of (a) 100, (b) 200, and (c) 300 A at the end of the simulation (at 2.65, 1.30, and 1.17 ms, respectively) shown along with the negative leader tip height versus time and the charge density ρ_z at the end of the simulation versus height. Peripheral branches which died out during the discharge tree development process and positive space streamer channels are shown in gray and green, respectively. The corresponding 3-D plots, additionally showing space stems and space charges forming the channel corona sheath are presented in Figure 5. Individual branches here and in Figure 5 are numbered, with this numbering being the same as in Tables 2 and C1-D1.

where $\sigma_m = 10^4$ S/m is the conductivity above which a channel segment is assumed to become essentially "immortal," even if no new links originated from it. Note that the initial link at the top of the downward extending discharge tree is set to be immortal (its conductivity is fixed at the level of 10^4 S/m).

Note that channel development and decay in our model may be occurring simultaneously in different parts of the discharge tree and that the number of links originating from the same parent node is limited to 26 (see Figure 2).

Simulation stops when a branch of the primary negative leader touches one of the boundaries of the cubical computational domain.

Key points of our leader development algorithm are given below:

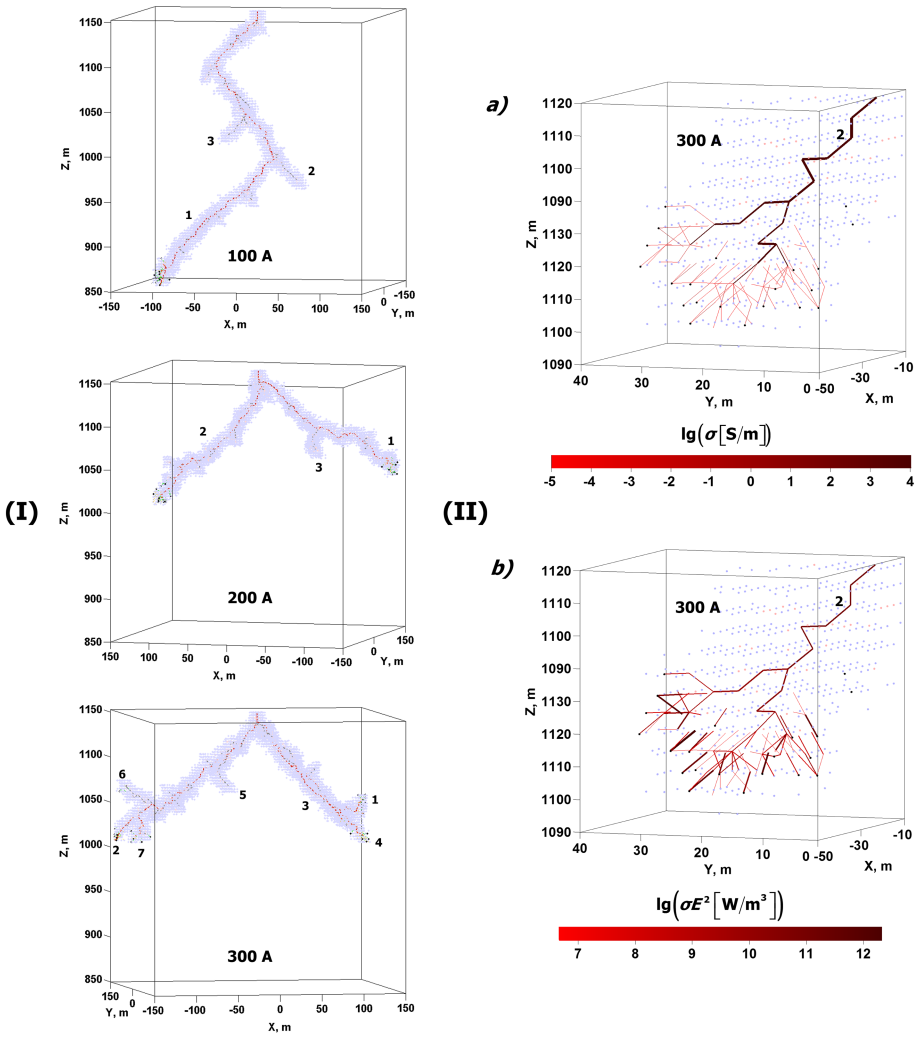

Figure 5. (I) Three-dimensional plots of three modeled negative stepped leaders with feeding currents of 100, 200, and 300 A at the end of the simulation (at 2.65, 1.30, and 1.17 ms, respectively). Peripheral branches that died out during the discharge tree development process and positive space streamer channels are shown in gray and green, respectively. Branch numbering is the same as in Figure 4 and in Tables 2 and D1-D3. Black dots denote space stems, and blue and pink dots (better seen in (II)) denote negative and positive space charges forming the leader channel corona sheath, respectively. (II) The lower part of the leader with the feeding current of 300 A at 319 μs (before the end of simulation at 1.17 ms) showing the fine structure of streamer formations near the leader tips. In (a) the color intensity represents electric conductivity of the channel, and in (b) it represents power density dissipated in the channel.

- Formation of a new link is accompanied by dipole-type charge separation. Initial conductivity of a newly formed link is set to 10^{-5} S/m.
- Conductivity of each link evolves in accordance with equation (8). Streamer link is assumed to transition to leader link when its conductivity exceeds the value of 1 S/m.
- Conductivity of links belonging to the negative leader streamer zone is limited to 1 S/m.
- Each link facilitates charge transfer via potential equalization current given by equation (10).
- Polarization of the overall discharge structure serves to relax the electric field in its interior and increase the electric field at its extremities (periphery).
- Each link either becomes part of the primary negative leader via the step formation process or decays with probability given by equation (11).
- Charges separated by decayed links remain "frozen" at the spatial grid nodes and become part of the negative leader channel corona sheath.

Table 1
Characteristics of Natural Negative Lightning Stepped Leaders Observed Using Photoelectric Systems and Framing Cameras

Study	Interstep interval (μs)	2-D step length[d](m)	2-D[a] leader speed (10^5 m/s)
Chen et al.[b](1999) (Australia)	5.0–50.0	7.9–19.8	4.5–11.2
Chen et al.[b](1999) (China)	18.0–21.0	8.5	4.9–5.8
Lu et al. (2008) (Florida)	0.2–15.7	—	15.0
Hill et al. (2011) (Florida)	12.2–40.0	4.8–7.1	2.7–6.2
Petersen and Beasley (2013) (Oklahoma)	—	—	5.6
Tran et al. (2014) (Florida)	—	14, 15	3.0
Qi et al. (2016) (China)	13.9-23.9	–	4.1–14.6
Jiang et al. (2017) (China)	6.9[c]	1.3-8.6	–

[a] Except for Petersen and Beasley (2013), who measured 1-D leader speed. [b] Studies based on the use of ALPS photoelectric system, as opposed to framing cameras used in all other studies summarized in this table. [c] Found as the observation period of 667 μs divided by the total number (96) of individual stepwise channel extensions. [d] For dart-stepped leaders, the step length is typically in the 5 to 10-m range (Idone & Orville, 1984; Gamerota et al., 2014).

3. Results

3.1. Discharge Tree Morphology

Figure 4 presents 2-D projections onto the *x-y*, *x-z*, and *y-z* planes of three modeled negative stepped leaders within roughly 1 km above ground with feeding currents of 100, 200, and 300 A. Also shown for each of the three events is the leader tip height above ground versus time and the line charge density ρ_z versus height. Figure 5 shows the three-dimensional negative leader channels, whose 2-D projections are seen in Figure 4, as well as the lower part of the leader with 300-A feeding current to better resolve the discharge activity near leader branch tips (channel segments are color-coded to show their electric conductivity or power density dissipated as heat).

The morphology of simulated leader channels shown in Figures 4 and 5 is similar to that seen in high-speed video images of negative lightning (Hill et al., 2011; Jiang et al., 2017; Lu et al., 2016; Petersen & Beasley, 2013; Qi et al., 2016; Tran et al., 2014). Specifically, note in Figure 5 (II) the multiple space streamers/leaders (mostly space streamers) simultaneously existing in the vicinity of each negative leader tip. Branching of the negative leader channel is caused by the random nature of space leader attachment to the primary channel, which is in agreement with recent optical observations reported by Tran et al. (2014) and Jiang et al. (2017). Space leaders which connected to the primary leader tip lengthened the existing channels, while those connected to the lateral surface of existing channels, created side branches. As seen in Figures 4 and 5, some leader channels exhibit substantial horizontal extent and even upward progression (for a short distance).

The number of model-predicted streamer channels/branches is larger than seen in optical records found in the literature. This can be explained by insufficient luminosity of most of the streamer channels, as noted in many studies (e.g., Hill et al., 2011; Petersen & Beasley, 2013; Qi et al., 2016; Rakov & Uman, 2003, pp. 135–136).

3.2. General Leader Characteristics

Quantitative characteristics of simulated leaders (see Tables 2 and D1-D3) are generally in good agreement with optical observations and inferred electrical parameters of stepped leaders. Characteristics of natural negative lightning stepped leaders observed using photoelectric systems and framing cameras found in the literature are summarized in Table 1. The large ranges of variation of the parameters presented in Table 1 can be largely attributed to the small number of leaders studied (only one or two in each of the papers listed in Table 1).

The extension speed of simulated negative leaders is of the order of 2×10^5 m/s (see Tables 2 and C1). Interstep intervals (see Table C2) vary in the range of 0.7–146.6 μs with a mean of 37.4 μs. Hill et al. (2011) reported the average interstep interval of about 20 μs from high-speed video recordings of natural lightning with interframe intervals of 3.33 μs. The mean step length (see Table C2) is of the order of 10 m. This is smaller than the typical step length of 50 m or so reported from older streak-camera observations (not included in Table 1),

Table 2
Characteristics of Negative Stepped Leaders Presented in Figures 4 and 5

Branch number	3-D extension speed[a] (10^5 m/s)	Space leader 3D length (m)	Number of steps		3-D interstep interval (μs)	3-D step length (m)	Charge transferred to the newly formed leader tip (mC)	The line charge density[b] (μC/m)
			Total	Time-resolved[c]				
				100 A feeding current				
1	2.14	4.9	90	71	29.1	9.0	1.99	369
2	1.88		8	6	44.0	8.8	1.92	524
3	2.27		5	5	46.2	8.9	1.83	504
				200 A feeding current				
1	2.23	4.9	35	31	36.3	9.1	2.04	379
2	2.33		47	37	26.4	8.8	1.92	408
3	2.15		6	6	43.8	9.2	1.99	563
				300 A feeding current				
1	2.72	5.0	45	34	24.2	9.2	1.88	325
2	2.70		53	38	21.6	9.1	2.05	406
3	1.81		11	11	51.8	8.8	2.01	398
4	2.11		9	9	45.7	8.9	2.01	346
5	2.20		7	7	43.2	8.6	2.11	493
6	2.62		6	6	41.2	9.1	1.88	524
7	2.75		6	4	32.7	9.1	1.94	442
Mean for all branches	2.30	4.9	25	20	37.4	9.0	1.97	437

[a] Leader speed for each individual branch (including only sections with conductivity exceeding 1 S/m) was calculated as its length divided by the time of its extension. [b] The line charge density of individual branches was calculated without double counting the nodes found in overlapping channel sheaths of two branches. [c]With 3.33-μs window (interframe interval used by Hill et al. (2011)).

but is within the range of more recently reported values, 1.3-20 m (see Table 1), obtained using framing cameras or ALPS. Possible reasons for the disparity in optically measured step lengths found in the literature were discussed by Hill et al. (2011). Note that optically measured step lengths are usually two-dimensional and, hence, are likely to be underestimated. The minimum step length in our model is limited by our 3-m grid spacing. We consider this adequate, because the overwhelming majority of the available data indicate that the minimum step length exceeds 3 m. The small number of reported step lengths in the 1.3 to 3 m range (about 10 out of 192 or <6% of the steps in the studies listed in Table 1) are apparently associated with unusual "alternate stepping of the branches sharing a root" (see Figures 3 and 5 of Jiang et al., 2017).

The line charge density of the simulated negative leader branches is about 400 μC/m (see Tables 2, C1, and D1). This is to be compared to 500 μC/m used in the simulations by Riousset et al. (2007) and 1, 000 μC/m experimantally estimated for negative stepped leaders by Proctor (1997). The aggregated line charge density along the vertical axis of simulated leader is of the order of 2, 000 μC/m (see Table C1). For comparison, the charge per unit length for the 300 m long pre–existing channel section (see Figure 1) was set to 800 μC/m. Note that each cell in Tables- 2 C2 and D1 contains two values corresponding to different approaches to counting steps. One value corresponds to all steps, including those responsible for the formation of minor branches (not numbered in Figures 4 and 5 and Tables 2 and C1-D1), and the other one (in the parentheses) is only for steps associated with extension of the numbered branches. More information about the negative stepped leaders presented in Figures 4 and 5 (I) can be found in Appendix D.

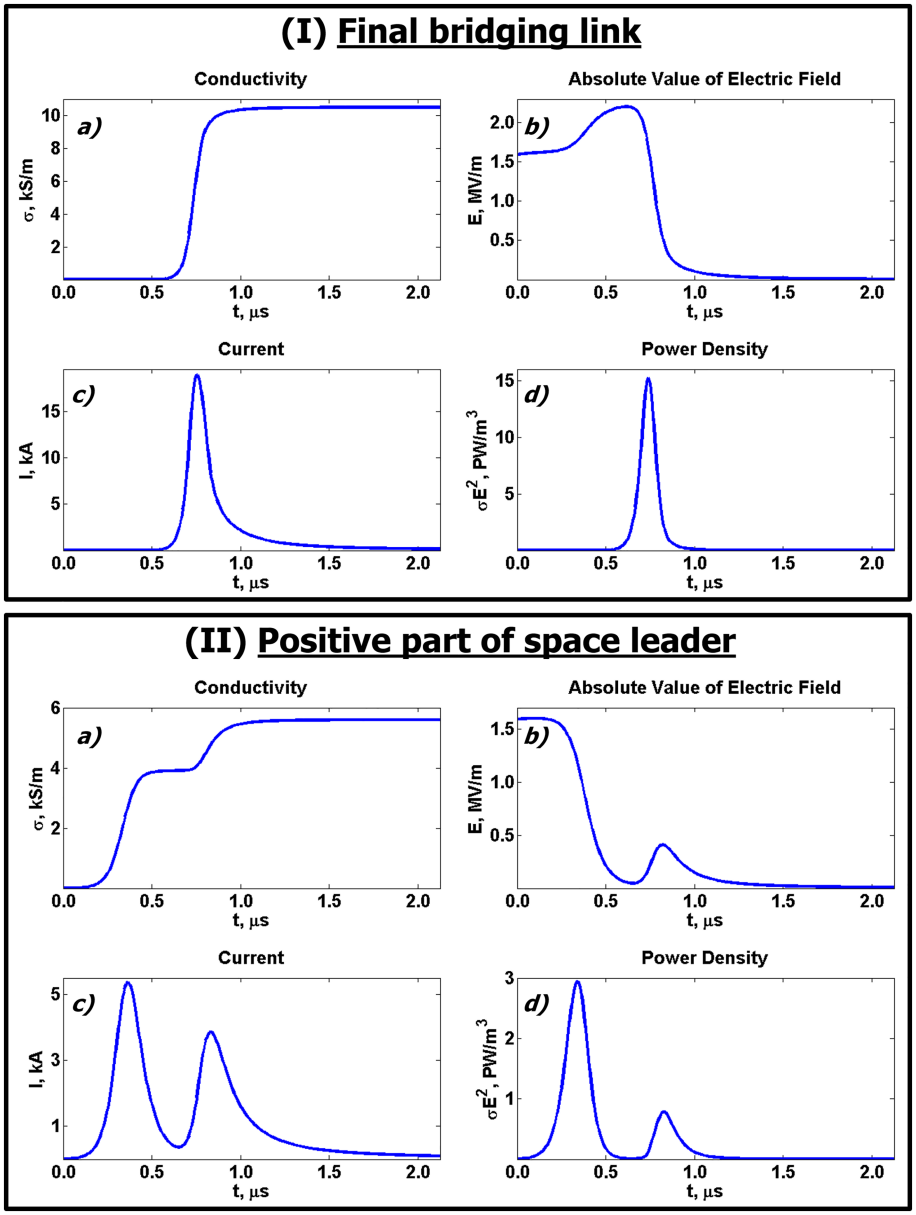

Figure 6. Typical temporal evolution during the step formation process of (a) conductivity, (b) absolute value of longitudinal electric field strength, (c) current, and (d) power density in the final link that bridged the space leader and primary leader channels (top panel labeled I) and in the positive part of space leader that originated from space stem (bottom panel labeled II). The feeding current was 200 A. The full time scale corresponds to one model time step (2.12 μs).

3.3. Step Formation Dynamics

Figure 6 shows a typical example of temporal evolution of conductivity, absolute value of longitudinal electric field strength, current, and power density in the channel section that linked the space leader to the primary leader; that is, in the final bridging link (the upper four panels) and in the positive part of space leader (the lower four panels), for the discharge with feeding current of 200 A.

Connection of space leader to the primary leader leads to a sharp increase of conductivity of the final bridging link, accompanied by longitudinal electric field reduction and sharp current and power density pulses, as expected for the step formation process. The time interval during which the significant changes in all the presented parameters occur is about 0.3–0.4 μs. The gradual increase of electric field prior to its more rapid decrease can be explained by charge accumulation at the ends of the poorly conducting streamer channel

section, which linked the space leader with the primary one. Once the conductivity of that link becomes sufficiently high, its electric field rapidly falls.

The minimum step current pulse peak and the minimum step charge transfer expected for negative lightning leaders are 2–8 kA and 1–4 mC, respectively (Krider et al., 1977). Nag and Rakov (2016) used the peak current of 10 kA near ground and 1 kA at higher altitudes in modeling negative stepped leaders. For the modeled event shown in Figure 6 (I), the step current peak and step charge are 18.9 kA and 2.1 mC, respectively. The conductivity of lightning leader channel core, according to Rakov and Uman (2003, p. 164), is similar to the typical arc conductivity of 10^4 S/m (10 kS/m). Our model-predicted conductivity is close to this value.

In contrast with the final bridging link, for the positive part of space leader (whose far end for the considered step became the newly formed negative leader tip) the temporal evolution of each of the examined quantities exhibits two stages. The first one (from 0 to 0.6 μs in Figure 6 (II)) corresponds to the time interval, during which the final bridging link connecting the space leader to the existing leader channel has insignificant conductivity and cannot provide potential equalization between the space and primary leaders. At this stage, the space leader channel continues to polarize as if it were unconnected with the primary one. The first current pulse with the peak of about 5 kA (occurring before the higher-current-peak pulse in Figure 6 (I)) reduces the longitudinal electric field strength and increases the channel conductivity from $\sim$ 1.5 MV/m to about 50 kV/m and from 1–10 S/m to 4 kS/m, respectively. As the final bridging link conductivity sharply rises at about 0.6 μs (see Figure 6 (I)), the second stage in Figure 6 (II) begins, at which the space leader actually becomes part of the primary leader channel. The relatively small electric field increase (hump) after 0.6 μs in Figure 6 (II)b is caused by charge redistribution between the two highly polarized leader sections, which transfers additional negative charge to the newly formed negative leader tip and equal amount of positive charge upward, potentially all the way to the initial node. This process is accompanied by a potential-equalization current pulse (the second pulse in Figure 6 (II)c), during which the final bridging link turns into a full-fledged part of the primary negative leader channel (see Figure 6 (I)). Note that the two-stage time evolution of quantities shown in Figure 6 (II) is typical for most of the space-leader channels involved in the step formation process, although time intervals between the two stages and relative magnitudes of the quantities corresponding to those stages may vary.

Similar two-stage development may take place in the lightning attachment process, which also includes the establishment of streamer connection (common streamer zone) between the downward and upward leaders of opposite polarities. It is likely that any connection in lightning and sparks occurs in two stages: streamer connection and hot-channel connection, each one being associated with a significant current rise (Tran & Rakov, 2017). In rocket-triggered lightning, streamer connection is associated with a current rise from some amperes to some hundreds of amperes (Hill et al., 2016), with hot leader channel connection occurring a couple of microseconds later and being associated with current rise to many kiloamperes. Sometimes between those two connections there are additional (attempted hot-channel) connections (see Tran & Rakov (2017) and references therein). Two current and light pulses have been documented during the attachment process in long negative sparks by Kostinskiy et al. (2016, Figures 2 and 4).

Figure 7 shows the current and power density waves in different sections of the channel associated with a single step presented in Figure 6. Three-dimensional distances between the center of each channel section and the newly formed leader tip are, from bottom to top, 6, 17, 58, 82, and 132 m. As one can see, a new negative leader step produces a sharp pulse (with 19 kA current peak), whose much reduced effect is felt hundreds of meters up along the channel. This behavior is qualitatively consistent with the propagation of step-luminosity pulses from the leader tip up along the channel reported by Wang et al. (1999) and Chen et al. (1999). We estimated the average values of the luminosity (power density) pulse speed to range from 7×10^7 to 8×10^7 m/s (not much different for feeding currents ranging from 100 to 300 A). Clearly, our model-predicted speeds are similar to the mean luminosity-pulse speed of 6.7×10^7 m/s reported by Wang et al. (1999). We also found that, disregarding the first 10–20 m, over which a very strong attenuation takes place, the typical distance over which a tenfold decrease in the power density peak occurs is about 30 m. For comparison, Wang et al. (1999) reported attenuation of luminosity peak to about 10% of the original (first recorded) value after traveling over a distance of 50 to 100 m. It is worth noting that the spatial resolution of ALPS used by Wang et al. (1999) did not allow them to adequately resolve all the steps (their height resolution was 30 m, and more than one step could occur within 30 m) and that they studied a dart-stepped leader, developing along the remnants of previously created channel.

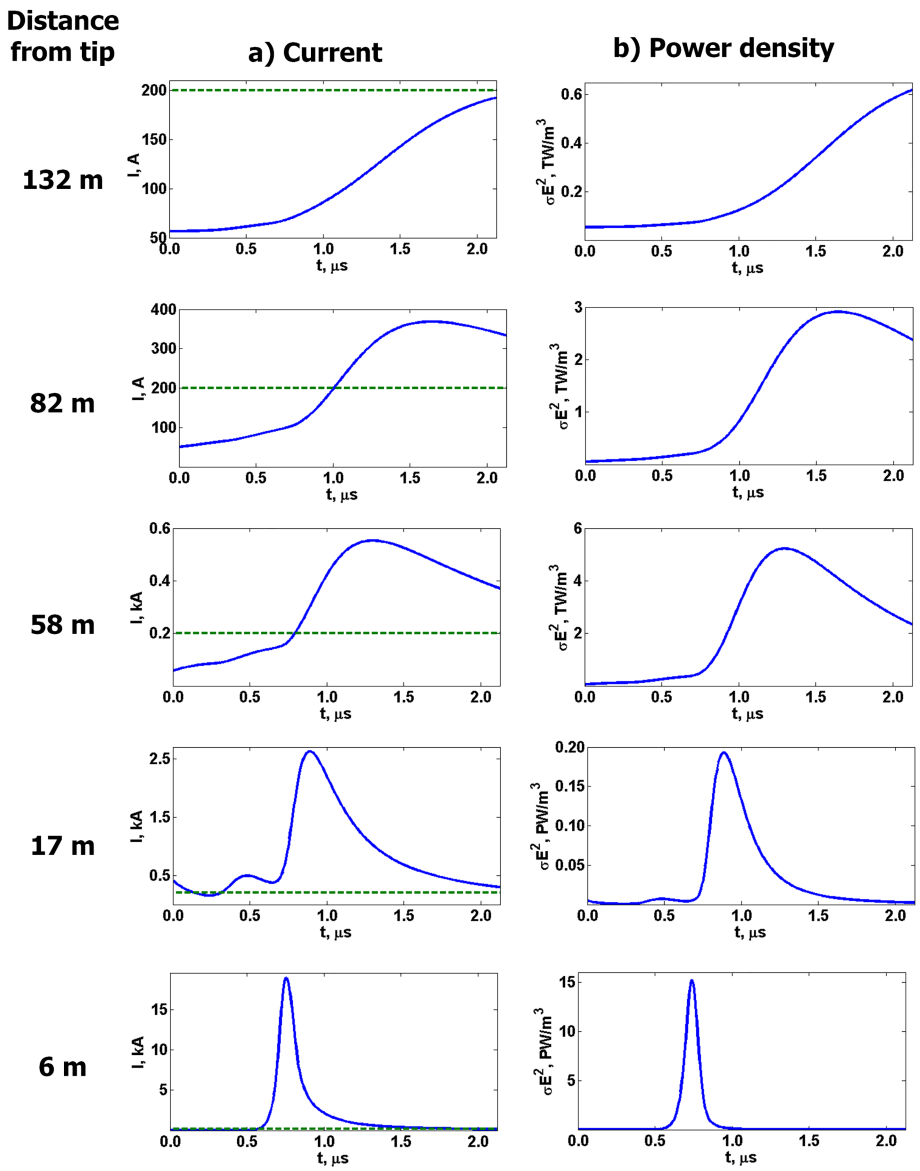

Figure 7. Temporal evolution of (a) current and (b) power density in different leader channel sections due to a single step for which the characteristics of final bridging link and positive part of space leader are presented in Figure 6. Green dashed lines in (a) show the value of feeding current, which was 200 A. Three-dimensional distances between the center of each channel section and the newly formed leader tip are, from bottom to top, 6, 17, 58, 82, and 132 m. The upward propagation speed of luminosity (power density) peak seen in this Figure between 6 and 82 m is about 8×10^7 m/s, and the peak at 82 m reduces to 1.5% of its value at 17 m. The panels labeled "6 m" are the same as the corresponding panels in Figure 6 (I). Note different vertical scales used at different distances from the tip.

3.4. Detailed Development Features

Table D2 presents information about the model-predicted space leader length and the dynamics of space stems, space streamers/leaders, and negative corona streamer bursts. The dynamics is represented by rates of occurrence of failed and successful space stems, space streamer/leader death, space leader making connection to the primary leader channel, and occurrence of negative streamers in the negative corona streamer burst. All the rates are given for the three leaders presented in Figures 4 and 5 (I) and are averaged over the entire simulation time. Our space leader lengths are in good agreement with those measured by Gamerota et al. (2014), who analyzed high-speed video recordings of dart-stepped leaders in triggered light-

ning. As one can see in Table D2, a very small fraction (1% and less than 5% with and without considering failed space stems, respectively) of space stems produce viable space leaders that make connection to the primary leader. The overwhelming majority of space stems produce only positive streamers that touch the primary leader channel and die, each leaving behind a pair of space charges. These space charges contribute to the formation of corona sheath, although their contribution is not dominant. Our simulations show (see Figure 4) that the dominant charge in the corona sheath is negative, and it is primarily supplied by negative corona streamer bursts.

Qi et al. (2016) observed three scenarios of space leader development: the space leader fails to make connection to the primary leader channel and eventually dies out (Scenario A), the space leader connects to the primary leader tip or its lateral surface via a low luminosity region (Scenario B), and the space leader connects to the primary leader channel forming a new step (Scenario C). All three scenarios introduced by Qi et al. (2016, Figure 8) were reproduced in our simulations.

Our simulation results also show how negative leader branches die out. Once a negative leader branch starts decaying, it is usually chocked by the space charge of its own corona sheath and can hardly recover and become active again. Indeed, the leader channel corona sheath charge reduces the electric field strength inside the sheath, which suppresses the growth of space leaders in its interior, so that they cannot reach the core of the branch and facilitate its extension. Once the branch dies out, space streamers/leaders continue to appear and die out at the periphery of the space-charge region created by the decayed branch. This process ends only when the electric field becomes insufficient to support space streamer/leader initiation and development. Similar processes take place during the negative corona streamer burst at the end of step formation process, when the newly formed negative leader tip abruptly emanates numerous negative streamers, whose charge reduces the electric field ahead of the leader tip.

The main physical parameter determining the overall negative leader morphology in our model is the magnitude of the feeding current I_b. It is clear from Figures 4 and 5 that a higher feeding current results in more numerous leader branches. Specifically, the leader with feeding current of 100 A had one major and two minor branches (a total of 3), while the corresponding numbers for leader branches with 200 and 300 A feeding currents were 2 and 1 (a total of 3) and 2 and 5 (a total of 7), respectively. These branches are numbered in Tables 2 and C1-D1 and Figures 4 and 5. There were also less significant branches (29, 31, and 40 for leaders with 100, 200, and 300 A feeding currents, respectively), most of which had relatively short lengths, of the order of 10 m, and relatively short lifetimes, of the order of tens of microseconds. It appears that, while the feeding current increases from 100 to 300 A, the average current per major branch remains about the same, at 100–150 A. For a higher feeding current the leader channel growth direction becomes less sensitive to the background (vertical in our case) electric field strength and is largely determined by the field of charges near the tip. Because of this, leaders with the feeding currents of 200 and 300 A have more pronounced horizontal extent compared to the leader with the feeding current of 100 A. It follows from Tables 2 and C1-D1 that most of the parameters of individual leader branches with the feeding currents of 100, 200, and 300 A are quite similar. These results suggest that, as the rate of charge supply to the leader channel increases, its branching becomes more likely, with individual branches repelling each other, and that the number of major branches is limited by the minimum current (100 A or so) required to keep the branch alive. The latter inferences are, of course, limited by the size of the computational domain used in this study and are in need of further investigation.

4. Discussion

A critical feature of our model is the polarity asymmetry (see Appendix A); that is, different initiation and propagation threshold fields for positive and negative streamers. Without this feature, our simulation results would not be in good agreement with the experimental data. Although the initiation field for positive streamers $E^+_{ith} = 1.34$ MV/m exceeds the propagation field $E^-_{pth} = 0.62$ MV/m for negative ones, for the field (1.43 MV/m) at which the probability of occurrence of a new floating (positive) channel is equal to 50% the probability of existing negative channel extension is only 37% (see Figure 3, red and green curves). As a result, at that field, it is easier to create a positive streamer originating from the space stem than to maintain the development of negative streamers from the primary leader channel tip. Thus, the main role in the step formation process is played by positive streamers originating from the space stem/leader, as the experimental data for long negative sparks suggest (e.g., Bazelyan & Raizer, 2000).

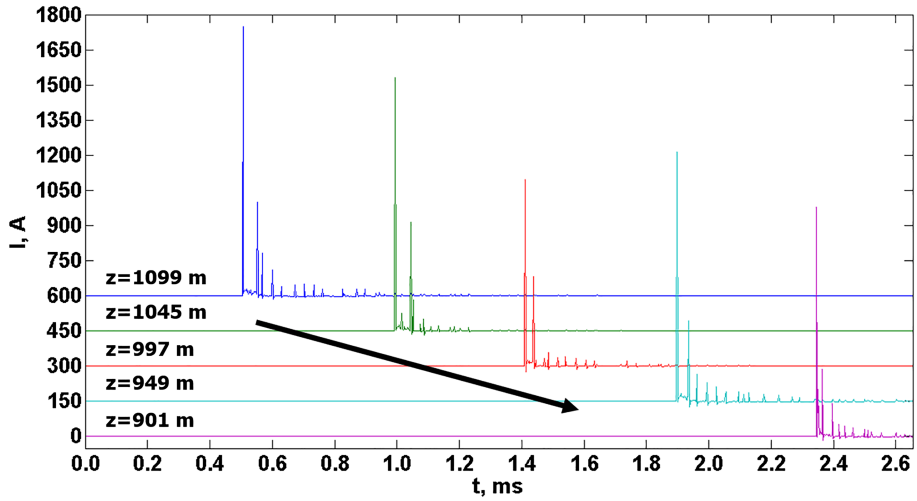

Figure 8. Transient leader current versus time waveforms at different heights, 901, 949, 997, 1,045, and 1,099 m above the ground for the feeding current of 100 A (the event shown in Figures 4a and 5 (I)). In each case, the initial (largest) current pulse is due to the step-formation process at the corresponding height. Plots for 949, 997, 1,045, and 1,099 m are shifted up by 150, 300, 450, and 600 A, respectively, for improved viewing. The positive sign of the current corresponds to upward motion of positive or downward motion of negative charge, expected for descending negative leaders. The negatively-sloped arrow indicates the overall downward progression of the leader tip at a 1-D speed of the order of 10^5 m/s.

It is important to note that we had to employ multiple thresholds for the same polarity, in order to achieve agreement with observations. Specifically, we had to distinguish between the first and subsequent (secondary) streamer channels originating from the space stem, in addition to different thresholds for initiation and propagation. Further studies are needed to better understand the need of multiple thresholds in our model.

Figure 8 shows the time variation of transient current flowing through the 5 primary negative leader channel nodes located at heights of 1099, 1045, 997, 949, and 901 m above the ground, for the event with feeding current of 100 A. Those nodes correspond to positions of negative leader tips formed at 0.50, 0.99, 1.41, 1.90, and 2.34 ms, respectively. The term "transient" means that this current is associated only with the charge variation occurring at specified nodes with the effect of feeding current removed. Note that the positive sign of the current corresponds to the upward motion of positive charge or the downward motion of negative charge (regardless of whether the charge of given sign enters or leaves the node), which is expected for descending negative leaders. The initial (large) current pulse at each height is associated with negative charge rapidly injected from the primary channel into the newly formed leader tip (or positive charge of the space leader injected into the primary leader channel), as a result of the step formation process at that height. This charge injection is also reflected in peaks (rapid fluctuations) in the vertical distribution of the line charge density in the negative leader channel (see Figure 4). The initial current pulse (occuring at a progressively later time as the height decreases) is followed by a sequence of smaller pulses. The latter (smaller) pulses correspond to the later-formed and progressively more distant (lower-altitude) leader steps. Figure 8 is qualitatively similar to the dart-stepped leader luminosity profiles seen in Figure 5 of Wang et al. (1999) and in Chen et al. (1999). Propagation of individual-step pulse from the leader tip up along the channel is shown in Figure 7. Note that the current pulses associated with steps can significantly exceed the feeding current (100 A). This is a result of large electric field (about 1–2 MV/m) between the tips of space and primary leaders at the beginning of the step formation process, which rapidly drops to the typical leader-channel internal field value of about 10 kV/m. This electric field reduction occurs in a very short time of about 0.1 μs (see Figure 6(I)b) and, hence, requires a very high electric current. It is important to note that the feeding current is responsible only for the magnitude of the negative charge injected in the simulation domain at each model time step and is not directly related to currents in individual branches belonging to the primary negative leader.

The results obtained in this study are significantly influenced not only by the choice of the model input parameters, the most influential of which are the threshold fields and the grid spacing, but also by relations (8) and (9), describing the channel conductivity evolution, and relation (11) specifying the probability

of channel decay. Those relations are somewhat subjective and tuned to achieve the expected results, which is unavoidable because of the complexity of processes being modeled. Clearly, there is a need for further experimental and theoretical studies to develop more accurate parameterizations. It is important to note that the high complexity of the step formation process does not allow one to evaluate many model-input parameters from the first principles. Because of this, one is forced to employ the trial-and-error method to search (using the results of sensitivity analysis as a guide) for the values of parameters that would allow a reasonable match between model outputs and observations. On the other hand, the proposed approach is useful in determining the ranges of model parameters, which allow one to satisfactorily describe the observed features of the negative lightning stepped leader development. Further, a generally good agreement of our model predictions with the bulk of optical and other observations of negative leaders suggests that the educated guesses we had to make on the number of free parameters and parametrizations in our model are representative of the physics involved.

5. Conclusion

A numerical model with physical timing and grid spacing of 3 m is applied to studying the progression (including stepping and branching) of negative lightning stepped leader. The asymmetry between positive and negative streamers is taken into account via using polarity-dependent initiation and propagation field thresholds. The stepped nature of negative leader is confirmed to be caused by this asymmetry. The step formation process of the negative leader is modeled to begin with the appearance of space stems inside and in the immediate vicinity of its streamer zone (corona streamer burst completing the preceding step). Some of those space stems evolve into space leaders, which can connect to the primary leader channel, thereby facilitating its extension.

It appears that space stems occur as a result of electric field intensification by the space charge rapidly pushed into the space ahead of the newly formed leader tip by the intense negative corona streamer burst, which completes the preceding step formation process.

Model-predicted morphology and dynamics of negative leaders are in good agreement with the results of recent observations of lightning stepped and dart-stepped leaders obtained using high-speed video cameras (Hill et al., 2011, Figures 1–4; Petersen & Beasley, 2013, Figures 1, 4, and 5; Gamerota et al., 2014, Figures 2–4; Tran et al., 2014, Figures 1 and 2; Lu et al., 2016, Figures 2–4, 6, and 7; Qi et al., 2016, Figures 1, 6, 7, and 9; Jiang et al., 2017, Figures 1–3). Among other things, the model reproduces branching, formation of space leaders, culmination of the step formation process in the corona streamer burst, and formation of negative corona sheath (this is best seen in Animations S1–S3 found in the supporting information). Further, the current and power density pulses generated as a result of step formation process in our model (see Figures 6 and 7) propagate upward from the newly formed leader tip in a manner similar to that reported by Wang et al. (1999, Figure 6) for a dart-stepped leader in rocket-triggered lightning. This result to some extent demonstrates the model predictive power, because the above feature cannot be readily achieved by straightforward adjustment of model-input parameters and it was not used in such adjustment. Current pulses generated at the end of step formation process carry positive charge over hundreds of meters upward along the negative leader channel. Those positive charge surges resemble return strokes in negative CGs, but occurring on a smaller scale. Also, the model-predicted electrical parameters are in line with the current knowledge on negative lightning leaders. All these observations (which are not all quantifiable) and parameters (most of which are found in Rakov and Uman (2003) and in references therein) serve as constraints for our model. Specifically, the following characteristics of negative stepped leader, which are in good agreement with experimental data, should be noted:

- the overall negative stepped leader extension speed is about 2.3×10^5 m/s, which is very close to the median 2-D speed, 2.2×10^5 m/s, optically measured for 62 leaders initiating first strokes in negative lightning by Campos et al. (2014);
- interstep intervals are in the range of 10–90 μs, which is consistent with typical interstep intervals of 16 and 25 μs measured in electric field records in Florida and Arizona, respectively, by Krider et al. (1977) and with the mean interstep intervals of 16 μs reported from optical records by Hill et al. (2011);
- the step length within 850–1350 m of ground is of the order of 10 m, which is in the range of values, 1.3–20 m, based on the photoelectric and framing-camera observations summarized in Table 1;

- the step charge is of the order of 2 mC, which is consistent with the 1–4 mC range estimated by Krider et al. (1977);
- the line charge density of individual branches is some hundreds of μC/m, which is comparable to the value of 1 mC/m estimated for negative stepped leaders by Proctor (1997);
- the speed of upward propagating power density pulse generated in the step formation process is in the range of 7×10^7 to 8×10^7 m/s, which is consistent with the mean 2-D speed of step- light pulses, 6.7×10^7 m/s, reported by Wang et al. (1999);
- Qi et al. (2016) observed three scenarios of space leader development: the space leader fails to make connection to the primary leader channel and eventually dies out (Scenario A), the space leader connects to the primary leader tip or its lateral surface via a low luminosity region (Scenario B), and the space leader connects to the primary leader channel forming a new step (Scenario C). All three scenarios introduced by Qi et al. (2016, Figure 8) were reproduced in our simulations.

We have also analysed supporting information of the sensitivity of our model to variation in model input parameters and found it to be sufficiently robust (see supporting information Text S6)

Appendix A: Polarity Asymmetry

All presently existing numerical models describing lightning discharge development (see, e.g., Davydenko & Iudin, 2016; Iudin & Davydenko, 2015; Iudin et al., 2015, 2017; Mansell et al., 2002, 2010; Riousset et al., 2007; Tan et al., 2006; Wang et al., 2016) do not consider the difference in fields required for propagation of positive and negative streamers. This polarity asymmetry is well known from laboratory spark studies, which indicate that the fields in streamer zones of positive and negative leaders, which are approximately constant, differ by about a factor of 2 and are equal to about 5 and 10 kV/cm, respectively (Gorin & Shkilev, 1976; Raizer, 2009, p. 596). It is reasonable to assume that the threshold fields for propagation of positive and negative streamers are close to the electric fields inside positive and negative leader streamer zones, respectively, and, hence, also differ by a factor of 2 or so. This inference is in general agreement with the modeling result obtained by Gallimberti et al. (2002), who theoretically examined the energy gain and loss at the streamer front and found that the magnitudes of stability fields corresponding to the energetically stable streamer propagation are 5 and 7.5 kV/cm for positive and negative streamers, respectively.

The polarity asymmetry is related to the difference in direction in which electrons move relative to the streamer head of each polarity. In a positive streamer, electrons produced in the vicinity of its head move toward it, so the ionization tends to happen in a stronger field. The head of negative streamer pushes electrons away (to a lower field region), so that ionization takes place under less favorable conditions (see, e.g., Bazelyan & Raizer, 2000, p. 84). In other words, a stronger field is required for development of negative streamers. The effect can be also related to the role of low-mobility positive space charge, which is produced in the tails of electron avalanches and serves to either enhance (positive streamer) or oppose (negative streamer) the external field in the forward direction. Further discussion of reasons for polarity asymmetry can be found in works of Williams (2006) and Kostinskiy et al. (2018).

Observations show that the streamer zone of positive leader in laboratory consists of positive streamers only (see, e.g., Bazelyan & Raizer, 2000, Figure 2.2). Extension of positive leaders in laboratory is optically continuous, at least when the absolute humidity is lower than $10\,g/m^3$ or so and the voltage impulse front is less than 1 ms or so (see Kostinskiy et al. (2018) and references therein). In lightning, both continuously moving and stepping positive leaders were observed (see, e.g., Rakov & Uman, 2003, p. 137, and references therein).

In contrast to positive leaders, the streamer zone of negative leader in long laboratory sparks and in lightning is complex and appears to consist of both negative and positive streamers (Bazelyan & Raizer, 2000; Gorin & Shkilev, 1976; Gamerota et al., 2014, p. 85). Further, negative leaders developing in virgin air are always stepped. During the step formation process, positive streamers extending from the space stem/leader toward the primary leader channel (in the backward direction) come in contact with negative streamers emanating from the primary leader tip. There are also negative streamers extending from the space stem/leader in the forward direction. When the positive end of space leader makes connection with the primary leader channel, the high potential of negative leader tip is rapidly transferred to the lower extremity of the space leader. This causes a powerful burst of negative corona streamers from the newly-formed negative leader tip that

was recently studied in detail by Kostinskiy et al. (2018). The streamer burst apparently creates conditions (highly nonuniform electric field) in which new space stems are born, with a potential to evolve into new steps.

In our model, we implement the negative leader stepping mechanism and use polarity-dependent electric field thresholds.

Appendix B: Charge Transport Renormalization Procedure

In this appendix, we discuss the method of feeding of (supplying negative charge to) the growing discharge tree in our model. Lightning leaders prior to their connection to the ground, have both positive and negative parts (see, e.g., Kostinskiy et al., 2015; van der Velde & Montanyà, 2013). The charge redistribution between those two parts occurs in such a way that the positive part acts as a source of negative charge for the negative one and vice versa. Since the entire discharge tree is to be electrically neutral, the negative charge transferred to the negative part by currents, given by (10), from the positive part must be equal in absolute value to the positive charge transferred to the positive part. In our model, the positive part is not simulated (see Figure 1), and charge is constantly supplied to the initial (upper) node of the negative part of the simulated discharge tree via the feeding current I_b. In this study, calculations were performed for three values of I_b, 100, 200, and 300 A, which are within the range of expected average negative lightning leader currents (Rakov & Uman, 2003, chapter 1.4, p. 7). Charge redistribution associated with currents given by (10) in all discharge tree links is normalized so that the current injecting positive charge into the initial node of the modeled negative leader from all discharge tree channels is equal to I_b. To avoid instability in the numerical scheme, this charge renormalization procedure takes place every $\tau_s = 1.42$ ns, where subscript "s" stands for small and is used to differentiate τ_s from the model time step $\tau = 2.12\,\mu s$, which is 1,500 times larger than τ_s. The intention here is to ensure that positive charge entering the initial node from the negative leader channel system below that node is compensated by the equal amount of negative charge supplied by feeding current I_b. One can view this charge renormalization as adjustment of the radii of negative leader channels to maintain the required potential equalization currents given by (10). At the same time, there is no recalculation of charge variation in the floating channels of space streamers/leaders. As a result, their channel radii can be viewed as constant. This algorithm allowed us to avoid (compensate for the nonphysical) charge accumulation at the initial node that is associated with the deposition of negative charge onto the extending negative leader channel.

As seen in Figure 1, the positive part of the discharge tree is replaced with an artificial feeder connected to the initial node of the negative part at the upper boundary of the computational domain. Because of that, the longitudinal electric field and conductivity of the initial channel segment in the computational domain are to be specified upfront We assumed that the initial channel segment is characterized by constant magnitudes of longitudinal electric field $E_b = 10^4$ V/m (see Bazelyan & Raizer, 2000, p. 204) and conductivity $\sigma_b = 10^4$ S/m (see Rakov & Uman, 2003, p. 164). Those values are typical for an established leader channel, which is similar to an electric arc. Calculations based on Ohm's law show that a leader channel with conductivity σ_b and longitudinal electric field E_b must have radii of the current-currying core of 0.56, 0.80, and 0.98 mm for the feeding currents I_b of 100, 200, and 300 A, respectively.

Appendix C: Simulation of Leader Stepping Mechanism

The sequence of processes involved in the formation of negative leader step is schematically shown in Figure C1. The leader stepping algorithm implemented in the model is as follows:

1. The negative corona streamer burst originating from the just-formed negative leader tip and completing the previous step formation process rapidly injects a large amount of negative charge into the space ahead of the leader tip. This streamer burst is seen at Stage A in Figure C1.
2. The injected space charge creates highly nonuniform electric field ahead of the negative leader tip. As a result, highly localized plasma seeds (space stems) are formed inside or near the negative space charge region (corona streamer burst). In Figure C1, three competing space stems are shown below the corona streamer burst at Stage B.

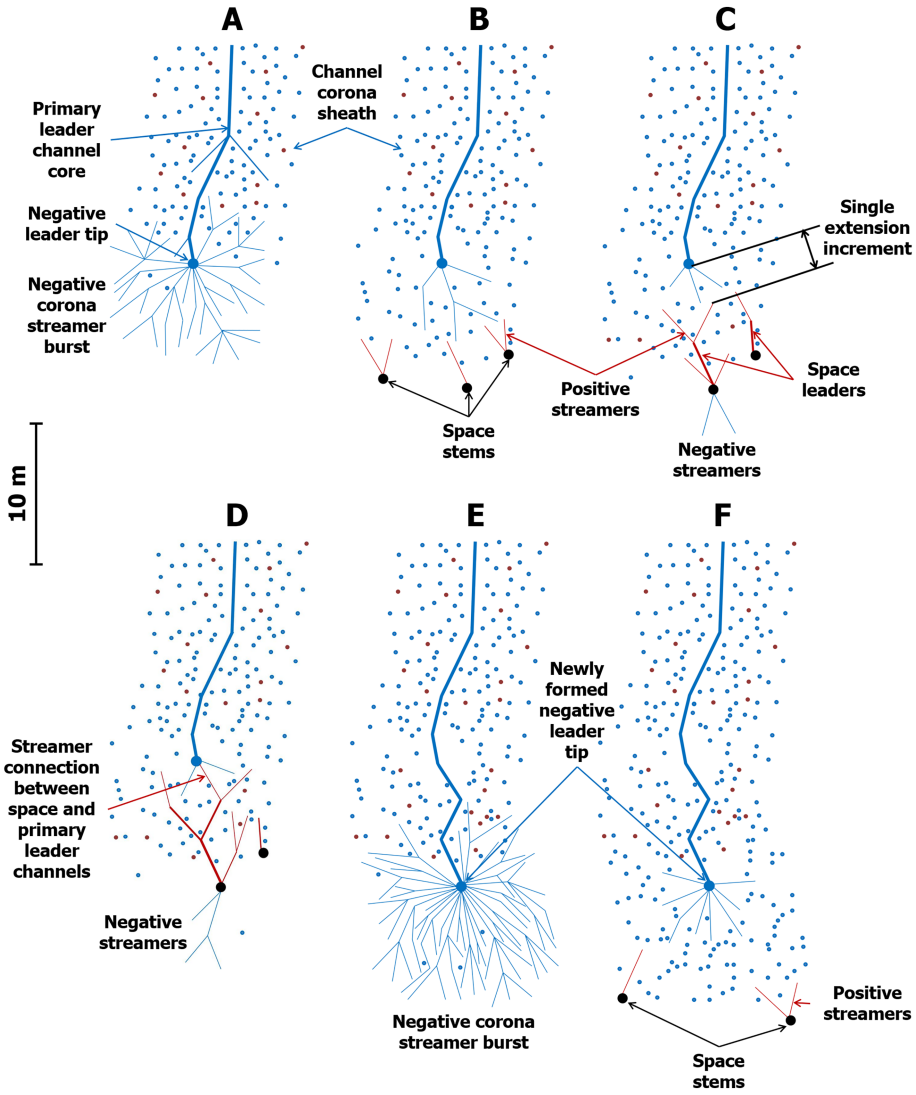

Figure C1. Schematic representation of the step formation process. The complete cycle (A–E) usually takes a few tens of microseconds. Red and blue colors correspond to positive and negative polarities, respectively, and black dots represent space stems. Thicker lines correspond to higher conductivities. Positive and negative space charges in the leader channel corona sheath are denoted by red and blue dots, respectively. The number of blue dots is considerably larger than the number of red dots, so that the net charge of corona sheath is negative.

3. Space stems launch positive streamers toward the primary negative leader channel, building up the potential for launching negative streamers in the opposite direction. As a result, bidirectional space streamer channels (collective space streamers) originating from the space stem are formed.
4. As the space streamer channels are heated by polarization current and their conductivity increases, they may become space leader channels. Since the positive part is formed earlier, it can reach the leader stage, while the negative part is still at the streamer stage or even absent. Both these scenarios are seen at Stage C in Figure C1. In the latter case (no negative streamers originating from the space stem), the charge is conserved by placing negative charge on the space stem as the positive part extends toward the primary channel. In our simulations, negative parts of space leaders never formed by the time of the space leader making connection to the primary leader channel.

   For simplicity, the following description refers to a single space leader.
5. The positive end of space streamer/leader channel moves toward the primary (negative) leader channel until the former comes within a single extension increment of the primary leader tip. This increment is labeled in the sketch of Stage C in Figure C1.

Table D1
Characteristics of Branches of the Negative Stepped Leaders Presented in Figures 4 and 5(I)

Branch number	3-D length (m)	Start time (μs)	End time[a] (μs)	Life time (μs)	3-D extension speed[b] (10^5 m/s)	Averaged 3-D interstep interval[c] (μs)	Line charge density (μC/m) 3-D[d]	1-D[e]
100 A feeding current								
1	568	0	2,654	2,654	2.14	24.6	394	886
2	58	1,409	2,556	1,147	1.88			
3	42	1,045	1,810	765	2.27			
200 A feeding current								
1	289	0	1,298	1,298	2.23	12.5	413	1,812
2	282	79	1,298	1,219	2.33			
3	47	552	1,049	497	2.15			
300 A feeding current								
1	305	0	1,173	1,173	2.72	7.4	370	2,451
2	303	51	1,173	1,122	2.70			
3	94	523	1,173	650	1.81			
4	77	795	1,173	378	2.11			
5	57	289	792	503	2.20			
6	54	846	1,173	327	2.62			
7	45	984	1,173	189	2.75			
Mean for all branches	171	—	—	—	2.30	14.8	392	1,716

[a] The end time for not decayed branches is determined by the end of simulation, which stops when one of the branches touches one of the boundaries of the simulation domain. [b] Leader speed for each individual branch (including only sections with conductivity exceeding 1 S/m) was calculated as its length divided by the time of its extension. [c] Averaged 3-D interstep intervals are calculated as the time interval between the appearance of the first step and the end of simulation divided by the total number of steps. [d] Leader charge per unit length is calculated as the absolute value of the ratio of the entire charge transferred into the simulation domain by the negative stepped leader to the total length of its branches (those, which are represented in the table) at the end of simulation. [e] The total charge transferred into the simulation domain per unit length along the z axis calculated under the assumption that the leader has a single vertical channel, the length of which is the difference between the heights of the simulation domain top (1,150 m) and the lowermost primary leader tip at the end of simulation.

6. If the floating channel segment separated from the primary leader tip by a gap equal to the single extension increment is sufficiently conducting (≥1 S/m), a new streamer link is placed between the positive end of that channel segment (space leader) and the primary (negative) leader channel. This link is labeled "Streamer connection between space and primary leader channels" in Figure C1 (see Stage D).
7. Connection of the floating space leader channel to the primary leader channel causes rapid rearrangement of charge distribution in the entire discharge tree, from the space stem (since in our simulations the negative part of space leader never formed by this time) to the initial node of primary negative leader. The resultant current heats all the channel segments that it traverses, so that their conductivity increases. The negative leader tip is transferred to the space stem from which the space leader originated, causing a negative corona streamer burst (see Stage E in Figure C1). The negative streamer channels (if any) originating from the space stem become elements of the negative corona streamer burst.
8. After Stage E, which is similar to Stage A, space stems are formed ahead of the new primary leader tip (see Stage F in Figure C1, which is similar to Stage B), and the step formation process repeats itself.

If at a given time, the electric field between a node that does not belong to the existing discharge structure, which we refer to as a potential space stem, and another (not necessarily free) node nearby exceeds

Table D2
Characteristics of Stepping of the Negative Stepped Leaders Presented in Figures 4 and 5 (I)

Branch number	Number of steps		3-D interstep interval (μs)			3-D step length (m)		
	Total	Time-resolved[a]	Min	Max	Mean	Min	Max	Mean
100 A feeding current								
1	90 (61)	71 (61)	0.7 (19.1)	104.1 (133.9)	29.1 (42.7)	7.2 (8.2)	10.4 (10.4)	9.0 (8.9)
2	8 (6)	6 (6)	0.7 (27.6)	97.7 (97.7)	44.0 (61.6)	7.2 (8.2)	10.4 (10.4)	8.8 (9.2)
3	5 (5)	5 (5)	29.7 (29.7)	74.4 (74.4)	46.2 (46.2)	8.2 (8.2)	9.4 (9.4)	8.9 (8.9)
200 A feeding current								
1	35 (29)	31 (29)	0.7 (23.4)	91.4 (102.0)	36.3 (43.0)	7.2 (7.2)	10.4 (10.4)	9.1 (9.2)
2	47 (29)	37 (29)	0.7 (19.1)	61.6 (97.7)	26.4 (41.8)	7.2 (8.2)	10.4 (10.4)	8.8 (9.0)
3	6 (4)	6 (4)	25.5 (33.4)	68.0 (99.9)	43.8 (64.4)	8.2 (8.2)	10.4 (10.4)	9.2 (9.1)
300 A feeding current								
1	45 (31)	34 (31)	0.7 (17.0)	63.7 (63.7)	24.2 (35.5)	8.2 (8.2)	10.4 (10.4)	9.2 (9.2)
2	53 (33)	44 (33)	0.7 (19.1)	61.6 (61.6)	21.6 (35.1)	7.2 (7.2)	10.4 (10.4)	9.1 (9.0)
3	11 (10)	11 (10)	25.5 (25.5)	87.1 (146.6)	51.8 (57.6)	7.2 (7.2)	10.4 (10.4)	8.8 (8.9)
4	9 (9)	9 (9)	23.4 (23.4)	68.0 (68.0)	45.7 (45.7)	8.2 (8.2)	10.4 (10.4)	8.9 (8.9)
5	7 (7)	7 (7)	23.4 (23.4)	89.2 (89.2)	43.2 (43.2)	8.2 (8.2)	9.4 (9.4)	8.6 (8.6)
6	6 (6)	6 (6)	31.9 (31.9)	55.2 (55.2)	41.2 (41.2)	7.2 (7.2)	10.4 (10.4)	9.1 (9.1)
7	6 (5)	4 (5)	2.1 (31.9)	44.6 (46.7)	32.7 (40.9)	8.2 (8.2)	9.4 (9.4)	9.1 (9.0)
Mean for all branches	25 (18)	21 (18)	12.7 (25.0)	74.4 (87.4)	37.4 (46.1)	7.7 (7.9)	10.2 (10.2)	9.0 (9.0)

Note. Each cell in Table C2 contains two values, one accounting for all steps associated with a given numbered branch (including those serving to form relevant unnumbered smaller branches) and the other one (in the parentheses) for the case of the steps associated with unnumbered branches ignored.
[a]With 3.33-?s window (interframe interval used by Hill et al. 2011).

the initiation threshold E_{ith}, then with the probability given by formula (5) a streamer link bridges these two nodes. Numerical estimates suggest that, during the discharge development process, the electric field at the position of prospective space stem increases approximately by a factor of 50 (relative to the background value) and is likely to exceed the threshold field $E_{ith}^{+} = 1.34$ MV/m in our model. Because of the polarity asymmetry (see Appendix A), a space stem always emits positive streamers first. The space stem can subsequently become the origin of other positive and negative streamers if the electric field between this and neighboring nodes exceeds the subsequent (secondary) initiation threshold fields $E_{s}^{+} = 0.67$ MV/m and $E_{s}^{-} = 0.81$ MV/m, respectively, which are set to be lower than the corresponding initiation threshold fields, but higher than the propagation ones. The ratio of positive to negative thresholds for subsequent initiation (0.83) is set to be larger than for first initiation (0.5) in order to promote initiation of subsequent negative streamers from the space stem. Note that we allow the streamer/leader links originating from the space stem to overlap the existing channels of the negative leader streamer zone. In the case of link overlapping, both links independently contribute to the current given by (10).

Positive streamers of the space leader often come in contact with the primary (negative) leader channel, but this does not always result in a new step. The necessary condition for step formation used in this study is a sufficiently high conductivity, assumed to be $\geq$1 S/m, on both sides of the final streamer link (streamer connection) bridging the space and primary leader channels (see Stage D in Figure C1). This can be viewed as a requirement that the links on both sides of the final streamer link are each at the leader stage of development. If this criterion is not met, the positive streamer link which came in contact with the negative leader channel dies out leaving behind the charges it caused to be transferred. Once the two channels whose conductivities are at least 1 S/m are connected via a streamer link with the initial conductivity $\sigma_0 = 10^{-5}$ S/m, it is assumed that the step formation process cannot be reversed.

At the end of each time step, all existing channel segments are divided into two categories. Included in the first category are only links between the initial (upper) node of the primary negative leader and the nodes corresponding to the space stems of space leaders, which were involved in formation of new steps that merged with the primary leader channel during this time step. Thus, the channel segments of the first type are those involved in the stepwise extension of the negative leader (potentially all the way up to the initial node) at this time step. All other channel segments are included in the second category. For each channel segment (regardless of its category) the conductivity and current are recalculated using formulas (8) and (10), respectively. As noted above, the charge variation, associated with current given by (10), occurs in the time interval $\tau_s = 1.42$ ns, which is much smaller than the model time step $\tau = 1,500\tau_s = 2.12$ μs. The conductivity of channels in the first category is recalculated 50 times, at every thirtieth small time step τ_s, while the conductivity of channels of the second type is recalculated only once, in the middle of the charge variation process. Since we use the same values of η' and β' in solving the recurrent equation (8) for channels of both categories, we, in effect, employ 50 times larger values of η' and β' for channels involved in the step formation process, conductivity of which is calculated 50 times more often. This is because in our model we deal with 3 m grid spacing, which does not allow us to correctly calculate the small-scale evolution of strong electric field pulse generated by the junction of a pair of leader channel segments of opposite polarity. The above procedure makes it possible to correctly reproduce the rapid heating of streamer link connecting the two leader sections, as well as the final transformation of space leader into an arc-like formation during the step formation process (see Figure 6). Note that the larger values of η' and β' do not affect the state of the primary leader channel segments, because they are all already at the leader stage. Any changes in the charge configuration at the end of each small time step ($\tau_s = 1.42$ ns) are accompanied by the electric potential recalculation using formula (1).

Any unconnected branches of the positive part of space leader (regardless of conductivity) are "switched off" at the time of that space leader making connection to the primary leader via the final streamer link. The charges residing on those unconnected branches contribute to the space charge of the leader channel corona sheath. Note that the net charge in the corona sheath is negative and that in our model this charge is almost exclusively associated with negative corona streamer bursts completing the step formation process (see Appendix A and Text S4 in the supporting information).

Appendix D: Detailed Characteristics of Simulated Negative Stepped Leaders

Here we present detailed characteristics of simulated negative stepped leaders shown in Figures 4 and 5 (I).

In Table C1, interstep intervals are calculated as the ratio of the leader lifetime to the total number of steps. This approach is justified when one cannot separate one branch from another. In Table C2, we present interstep intervals for individual branches, which are more accurate than those given in Table C1.

In Table C1, the line charge density is calculated as the ratio of the total space charge to the total length of all leader branches. In Table D1, we present the line charge density for individual branches considering regions, where corona sheaths of two or more channels overlap.

Note that such step parameters as the transferred charge, current peak, and final channel conductivity vary significantly for different steps. They are mainly determined by the local electric field configuration at the

Table D3
Electrical Characteristics of the Negative Leaders Shown in Figures 4 and 5 (I)

Branch number	Final channel conductivity[a](kS/m)			Current peak value[a](kA)			Charge transferred to the newly formed leader tip (mC)			Line charge density, (μC/m)
	Min	Max	Mean	Min	Max	Mean	Min	Max	Mean	
100 A feeding current										
1	8.50	(20.00)	17.74	2.61	31.23	15.96	0.92	2.53	1.99	
	(13.83)	20.00	(18.87)	(7.28)	(31.23)	(18.09)	(1.59)	(2.53)	(2.12)	369
2	11.36	20.00	16.29	5.49	21.64	12.90	1.53	2.35	1.92	
	(14.19)	(20.00)	(17.50)	(9.70)	(21.64)	(15.01)	(1.59)	(2.35)	(2.01)	524
3	7.97	19.63	16.08	2.36	16.20	12.24	1.12	2.15	1.83	
	(7.97)	(19.63)	(16.08)	(2.36)	(16.20)	(12.24)	(1.12)	(2.15)	(1.83)	504
200 A feeding current										
1	4.40	13.22	9.75	3.15	29.78	17.30	0.96	2.52	2.04	
	(5.11)	(12.42)	(9.99)	(4.80)	(29.78)	(17.47)	(0.96)	(2.52)	(2.09)	379
2	3.15	12.76	8.91	1.79	27.08	13.99	0.93	2.40	1.92	
	(5.89)	(12.76)	(9.56)	(5.60)	(27.08)	(15.92)	(1.38)	(2.40)	(2.02)	408
3	8.90	10.35	9.54	14.22	16.74	15.47	1.92	2.11	1.99	
	(9.46)	(10.35)	(9.86)	(14.73)	(16.54)	(15.46)	(1.92)	(2.11)	(2.01)	563
300 A feeding current										
1	2.85	7.94	5.49	3.79	25.29	12.25	1.23	2.43	1.88	
	(4.00)	(7.94)	(5.83)	(5.68)	(25.29)	(13.51)	(1.39)	(2.43)	(1.96)	325
2	4.5×10^{-3}	8.95	6.32	0.01	29.96	15.55	1.3×10^{-4}	2.72	2.05	
	(4.07)	(8.95)	(6.55)	(6.14)	(29.96)	(16.31)	(1.61)	(2.72)	(2.12)	406
3	3.89	7.55	6.36	6.66	22.49	16.56	1.35	2.28	2.01	
	(3.89)	(7.55)	(6.55)	(6.66)	(22.49)	(17.24)	(1.35)	(2.28)	(2.05)	398
4	5.17	7.68	6.38	11.21	22.29	16.70	1.71	2.24	2.01	
	(5.17)	(7.68)	(6.38)	(11.21)	(22.29)	(16.70)	(1.71)	(2.24)	(2.01)	346
5	5.89	7.18	6.58	12.29	19.20	16.20	1.97	2.18	2.11	
	(5.89)	(7.18)	(6.58)	(12.29)	(19.20)	(16.20)	(1.97)	(2.18)	(2.11)	493
6	3.12	6.79	5.47	3.71	20.18	13.53	1.25	2.18	1.88	
	(3.12)	(6.79)	(5.47)	(3.71)	(20.18)	(13.53)	(1.25)	(2.18)	(1.88)	524
7	4.62	6.99	5.92	7.87	17.64	14.30	1.67	2.08	1.94	
	(5.57)	(6.99)	(6.18)	(12.06)	(17.64)	(15.59)	(1.84)	(2.08)	(2.00)	442
Mean for all branches	5.37	11.46	9.29	5.78	23.06	14.84	1.27	2.32	1.97	
	(6.78)	(11.40)	(9.65)	(7.86)	(23.04)	(15.64)	(1.51)	(2.32)	(2.02)	437

Note. Each cell in Table D1 contains two values, one accounting for all steps associated with a given numbered branch (including those serving to form relevant unnumbered smaller branches) and the other one (in the parentheses) for the case of the steps associated with unnumbered branches ignored.
[a] The magnitudes of final channel conductivity and current peak are given for the final bridging link between the space leader and primary leader channels.

Table D4
Characteristics of Space Streamers/Leaders and Negative Corona Streamer Bursts in Three Leaders Presented in Figures 4 and 5 (I)

Feeding current (A)	Space leader 3-D length (m)			Rate of failed space stem occurrence (10^6 s^{-1})	Rate of successful space stem occurrence (10^6 s^{-1})	Rate of space streamer /leader death (10^6 s^{-1})	Rate of space leader connection to the primary channel (10^3 s^{-1})	Rate of occurrence of negative streamers in corona streamer burst[b] and [c] (10^6 s^{-1})
	Min[a]	Max	Mean					
100	4.2	5.2	4.9	3.53	1.00	0.95	40.70	3.71 (7.01)
200	4.2	5.2	4.9	6.44	1.73	1.63	80.12	6.23 (12.74)
300	3.0	5.2	5.0	9.48	2.66	2.50	134.72	9.41 (19.29)
Mean	3.8	5.2	4.9	6.48	1.80	1.69	85.18	6.45 (13.01)

[a] Limited by grid spacing (3 m). [b] All negative streamers are assumed to eventually die. [c] In each cell, the smaller value corresponds to negative streamer channels originating directly from the negative leader tip or leader channel surface, while the larger one (in the parentheses) is for the total number of negative streamer channels, which additionally includes those originating from the previously created negative streamer channels, that is, not having direct connection with the primary leader channel. Streamer channels are defined here as those having conductivity lower than 1 S/m.

moment of connection of space leader to the primary leader channel. It is clear from Table D1 that the final conductivities of the final bridging links between the space leader and primary leader channels are about twice higher for the feeding current of 100 A than for feeding currents of 200 and 300 A. This is probably because of relatively small number of space streamers/leaders for the relatively low feeding current of 100 A, which results in a less significant electric field reduction along the bridging streamer link and, as a consequence, higher final conductivity of that link. Conversely, for higher feeding currents, there is a larger number of space streamers/leaders (see Table D2), which serves to more effectively relax the electric field in the vicinity of the negative leader tip, leading to a lower final conductivity of the bridging link. As each conducting link results in a decrease of electric field between the pair of nodes it bridges, a denser network of conducting links, which forms for a higher feeding current, corresponds to a lower electric field inside the volume occupied by that network.

Acknowledgments
This work was supported in part by the Russian Science Foundation (Project 19-17-00183). The authors express their gratitude to S. S. Davydenko and N. A. Popov for productive discussions on the subject of this study. Useful comments were provided by E. R. Mansell and anonymous reviewers. According to the AGU Publications Data Policy, the data presented in this paper are placed in a public domain repository (https://doi.org/10.5281/zenodo.3483194).

References

Allen, N. L., & Mikropoulos, P. N. (1999). Dynamics of streamer propagation in air. *Journal of Physics D: Applied Physics*, *32*(8), 913.
Bacchiega, G. L., Gazzani, A., Bernardi, M., Gallimberti, I., & Bondiou-Clergerie, A. (1994). Theoretical modelling of the laboratory negative stepped-leader. ICOLSE.
Bazelyan, J. M., & Raizer, Y. P. (2000). *Lightning physics and lightning protection*. Bristol, Philadelphia: Institute of Physics Publishing.
Campos, L. Z. S., Saba, M. M. F., Warner, T. A., Pinto, O., Krider, E. P., & Orville, R. E. (2014). High-speed video observations of natural cloud-to-ground lightning leaders a statistical analysis. *Atmospheric Research*, *135-136*, 285–305.
Carlson, B. E., Liang, C., Bitzer, P., & Christian, H. (2015). Time domain simulations of preliminary breakdown pulses in natural lightning. *Journal of Geophysical Research: Atmospheres*, *120*, 5316–5333. https://doi.org/10.1002/2014JD022765
Chen, M., Takagi, N., Watanabe, T., Wang, D., Kawasaki, Z.-I., & Liu, X. (1999). Spatial and temporal properties of optical radiation produced by stepped leaders. *Journal of Geophysical Research*, *104*(D22), 27,573–27,584. https://doi.org/10.1029/1999JD900846
Cooray, V., & Arevalo, L. (2017). Modeling the stepping process of negative lightning stepped leaders. *Atmosphere*, *8*(12), 245. https://doi.org/10.33902/atmos8120245
da Silva, C. L., & Pasko, V. P. (2015). Physical mechanism of initial breakdown pulses and narrow bipolar events in lightning discharges. *Journal of Geophysical Research: Atmospheres*, *120*, 4989–5009. https://doi.org/10.1002/2015JD023209
Davydenko, S. S., & Iudin, D. I. (2016). Fractal model of a compact intracloud discharge. II. Specific features of electromagnetic emission. *Radiophysics and Quantum Electronics*, *59*(7), 560–575. https://doi.org/10.1007/s11141-016-9723-5
Dulzon, A. A., Lopatin, V. V., Noskov, M. D., & Pleshkov, O. L. (1999). Modelling the development of the stepped leader of a lightning discharge. *Technical Physics*, *44*(4), 394–398.
Gallimberti, I., Bacchiega, G., Bondiou-Clergerie, A., & Lalande, P. (2002). Fundamental processes in long air gap discharges. *Comptes Rendus Physique*, *3*(10), 1335–1359.
Gamerota, W. R., Idone, V. P., Uman, M. A., Ngin, T., Pilkey, J. T., & Jordan, D. M. (2014). Dart-stepped-leader step formation in triggered lightning. *Geophysical Research Letters*, *41*, 2204–2211. https://doi.org/10.1002/2014GL059627
Gorin, B. N., & Shkilev, A. V. (1976). The development of electrical discharge in long gaps rod-plane with a negative voltage pulse. *Elektrichestvo (in Russian)*, *6*, 31–39.
Hill, J. D., Uman, M. A., & Jordan, D. M. (2011). High-speed video observations of a lightning stepped leader. *Journal of Geophysical Research*, *116*, D16117. https://doi.org/10.1029/2011JD015818

Hill, J. D., Uman, M. A., Jordan, D. M., Ngin, T., Gamerota, W. R., Pilkey, J., & Caicedo, J. (2016). The attachment process of rocket-triggered lightning dart-stepped leaders. *Journal of Geophysical Research: Atmospheres*, *121*, 853–871. https://doi.org/10.1002/2015JD024269

Idone, V. P., & Orville, R. E. (1984). Three unusual strokes in a triggered lightning flash. *Journal of Geophysical Research*, *89*, 7311–16.

Iudin, D. I., & Davydenko, S. S. (2015). Fractal model of a compact intracloud discharge. I. Features of the structure and evolution. *Radiophysics and Quantum Electronics*, *58*(7), 477–496. https://doi.org/10.1007/s11141-015-9621-2

Iudin, D. I., Iudin, F. D., & Hayakawa, M. (2015). Modeling of the intracloud lightning discharge radio emission. *Radiophysics and Quantum Electronics*, *58*(3), 173–184. https://doi.org/10.1007/s11141-015-9591-4

Iudin, D. I., Rakov, V. A., Mareev, E. A., Iudin, F. D., Syssoev, A. A., & Davydenko, S. S. (2017). Advanced numerical model of lightning development: Application to studying the role of LPCR in determining lightning type. *Journal of Geophysical Research: Atmospheres*, *122*, 6416–6430. https://doi.org/10.1002/2016JD026261

Jiang, R., Qie, X., Zhang, H., Liu, M., Sun, Z., Lu, G., et al. (2017). Channel branching and zigzagging in negative cloud-to-ground lightning. *Scientific Reports*, *7*(1), 3457. https://doi.org/10.1038/s41598-017-03686-w

Kostinskiy, A. Y., Syssoev, V. S., Bogatov, N. A., Mareev, E. A., Andreev, M. G., Bulatov, M. U., et al. (2016). Observations of the connection of positive and negative leaders in meter-scale electric discharges generated by clouds of negatively charged water droplets. *Journal of Geophysical Research: Atmospheres*, *121*, 9756–9766. https://doi.org/10.1002/2016JD025079

Kostinskiy, A. Y., Syssoev, V. S., Bogatov, N. A., Mareev, E. A., Andreev, M. G., Bulatov, M. U., et al. (2018). Abrupt elongation (stepping) of negative and positive leaders culminating in an intense corona streamer burst: Observations in long sparks and implications for lightning. *Journal of Geophysical Research: Atmospheres*, *123*, 5360–5375. https://doi.org/10.1029/2017JD027997

Kostinskiy, A. Y., Syssoev, V. S., Bogatov, N. A., Mareev, E. A., Andreev, M. G., Makalsky, L. M., et al. (2015). Infrared images of bidirectional leaders produced by the cloud of charged water droplets. *Journal of Geophysical Research: Atmospheres*, *120*, 10,728–10,735. https://doi.org/10.1002/2015JD023827

Krider, E., Weidman, C., & Noggle, R. C. (1977). The electric field produced by lightning leader steps. *Journal of Geophysical Research*, *82*(6), 951–960.

Lu, W., Qi, Q., Wang, D., Chen, L., Rakov, V. A., Ma, Y., et al. (2016). Two basic leader connection scenarios observed in negative lightning attachment process. *High Voltage*, *1*(1), 11–17. https://doi.org/10.1049/hve.2016.0002

Lu, W., Wang, D., Takagi, N., Rakov, V., Uman, M., & Miki, M. (2008). Characteristics of the optical pulses associated with a downward branched stepped leader. *Journal of Geophysical Research*, *113*, D21206. https://doi.org/10.1029/2008JD010231

Luque, A., & Ebert, U. (2014). Growing discharge trees with self-consistent charge transport: The collective dynamics of streamers. *New Journal of Physics*, *16*(1), 013,039.

MacGorman, D. R., & Rust, W. D. (1998). *The electrical nature of thunderstorms*. New York: Oxford Univ. Press.

Mansell, E. R., MacGorman, D. R., Ziegler, C. L., & Straka, J. M. (2002). Simulated three-dimensional branched lightning in a numerical thunderstorm model. *Journal of Geophysical Research*, *107*(D9), ACL 2–1–ACL 2–12. https://doi.org/10.1029/2000JD000244

Mansell, E. R., Ziegler, C. L., & Bruning, E. C. (2010). Simulated electrification of a small thunderstorm with two-moment bulk microphysics. *Journal of the Atmospheric Sciences*, *67*(1), 171–194. https://doi.org/10.1175/2009jas2965.1

Maslowski, G., & Rakov, V. A. (2006). A study of the lightning channel corona sheath. *Journal of Geophysical Research*, *111*, D14110. https://doi.org/10.1029/2005jd006858

Nag, A., & Rakov, V. A. (2016). A unified engineering model of the first stroke in downward negative lightning. *Journal of Geophysical Research: Atmospheres*, *121*, 2188–2204. https://doi.org/10.1002/2015JD023777

Ortega, P., Domens, P., Gibert, A., Hutzler, B., & Riquel, G. (1994). Performance of a 16.7 m air rod-plane gap under a negative switching impulse. *Journal of Physics D: Applied Physics*, *27*(11), 2379–2387. https://doi.org/10.1088/0022-3727/27/11/019

Petersen, D. A., & Beasley, W. H. (2013). High-speed video observations of a natural negative stepped leader and subsequent dart-stepped leader. *Journal of Geophysical Research: Atmospheres*, *118*, 12,110–12,119. https://doi.org/10.1002/2013JD019910

Phelps, C. T. (1974). Positive streamer system intensification and its possible role in lightning initiation. *Journal of Atmospheric and Solar-Terrestrial Physics*, *36*, 103–111.

Proctor, D. E. (1997). Lightning flashes with high origins. *Journal of Geophysical Research*, *102*(D2), 1693–1706. https://doi.org/10.1029/96JD02635

Qi, Q., Lu, W., Ma, Y., Chen, L., Zhang, Y., & Rakov, V. A. (2016). High-speed video observations of the fine structure of a natural negative stepped leader at close distance. *Atmospheric Research*, *178-179*, 260–267. https://doi.org/10.1016/j.atmosres.2016.03.027

Raizer, Y. P. (2009). *Gas discharge physics (in russian)*. Dolgoprudny: Intellect.

Rakov, V. A. (1998). Some inferences on the propagation mechanisms of dart leaders and return strokes. *Journal of Geophysical Research*, *103*(D2), 1879–1887. https://doi.org/10.1029/97JD03116

Rakov, V. A., & Uman, M. A. (2003). *Lightning: Physics and effects*. New York: Cambridge University Press.

Reess, T., Ortega, P., Gibert, A., Domens, P., & Pignolet, P. (1995). An experimental study of negative discharge in a 1.3 m point-plane air gap: The function of the space stem in the propagation mechanism. *Journal of Physics D: Applied Physics*, *28*(11), 2306–2313.

Riousset, J. A., Pasko, V. P., Krehbiel, P. R., Thomas, R. J., & Rison, W. (2007). Three-dimensional fractal modeling of intracloud lightning discharge in a New Mexico thunderstorm and comparison with lightning mapping observations. *Journal of Geophysical Research*, *112*, D15203. https://doi.org/10.1029/2006JD007621

Rompe, R., & Weizel, W. (1944). Über das toeplersche funkengesetz. *Zeitschrift für Physik*, *122*(9-12), 636–639. https://doi.org/10.1007/bf01330625

Sadiku, M. N. O. (2018). *Elements of electromagnetics*. Oxford: Oxford University Press.

Tan, Y., Tao, S., & Zhu, B. (2006). Fine-resolution simulation of the channel structures and propagation features of intracloud lightning. *Geophysical Research Letters*, *33*, L09809. https://doi.org/10.1029/2005gl025523

Tran, M. D., & Rakov, V. A. (2017). A study of the ground-attachment process in natural lightning with emphasis on its breakthrough phase. *Scientific Reports*, *7*(1), 15,761. https://doi.org/10.1038/s41598-017-14842-7

Tran, M. D., Rakov, V. A., & Mallick, S. (2014). A negative cloud-to-ground flash showing a number of new and rarely observed features. *Geophysical Research Letters*, *41*, 6523–6529. https://doi.org/10.1002/2014gl061169

van der Velde, O. A., & Montanyà, J. (2013). Asymmetries in bidirectional leader development of lightning flashes. *Journal of Geophysical Research: Atmospheres*, *118*, 13,504–13,519. https://doi.org/10.1002/2013JD020257

Wang, H., Guo, F., Zhao, T., Qin, M., & Zhang, L. (2016). A numerical study of the positive cloud-to-ground flash from the forward flank of normal polarity thunderstorm. *Atmospheric Research*, *169*, 183–190. https://doi.org/10.1016/j.atmosres.2015.10.011

Wang, D., Takagi, N., Watanabe, T., Rakov, V. A., & Uman, M. A. (1999). Observed leader and return-stroke propagation characteristics in the bottom 400 m of a rocket-triggered lightning channel. *Journal of Geophysical Research*, *104*(D12), 14,369–14,376. https://doi.org/10.1029/1999JD900201

Williams, E. R. (2006). Problems in lightning physics—The role of polarity asymmetry. *Plasma Sources Science and Technology*, *15*(2), S91.
Yos, J. M. (1963). Transport properties of nitrogen, hydrogen, oxygen, and air to 30,000 K. Tech. Memo RAD-TM-63-7, Contract AF33(616)-7578, Task 73603, 1–62.
Zhang, X., Zhu, Y., Gu, S., & He, J. (2017). Dynamics of branching of negative downward lightning leaders. *Applied Physics Letters*, *111*(22), 224,101. https://doi.org/10.1063/1.5010714